cells

MDPI

Article

From Brain to Blood: Uncovering Potential Therapeutical Targets and Biomarkers for Huntington's Disease Using an Integrative RNA-Seq Analytical Platform (BDASeq®)

João Rafael Dias Pinto [1,2], Benedito Faustinoni Neto [1], Luciana Munhoz [3], Irina Kerkis [4,*] and Rodrigo Pinheiro Araldi [1,2,*]

[1] BioDecision Analytics Ltd., São Paulo 01451-917, SP, Brazil; joao.dias@biodecesionanalytics.com (J.R.D.P.); bfaustinoni@gmail.com (B.F.N.)
[2] Post-Graduation Program in Structural and Functional Biology, Paulista School of Medicine, Federal University of São Paulo (UNIFESP), São Paulo 04023-062, SP, Brazil
[3] Brazilian Huntington Disease Union House, Scientific Committee, São Paulo 01320-010, SP, Brazil; dra.lucimunhoz@usp.br
[4] Genetics Laboratory, Butantan Institute, São Paulo 05503-900, SP, Brazil
* Correspondence: irina.kerkis@butantan.gov.br (I.K.); rodrigo.araldi@biodecisionanalytics.com (R.P.A.); Tel.: +55-11-2627-9701 (I.K.)

Abstract

Background: Huntington's Disease (HD) remains without disease-modifying treatments, with existing therapies primarily targeting chorea symptoms and offering limited benefits. This study aims to identify druggable genes and potential biomarkers for HD, focusing on using RNA-Seq analysis to uncover molecular targets and improve clinical trial outcomes. Methods: We reanalyzed transcriptomic data from six independent studies comparing cortex samples of HD patients and healthy controls. The Propensity Score Matching (PSM) algorithm was applied to match cases and controls by age. Differential expression analysis (DEA) coupled with machine learning algorithms were coupled to identify differentially expressed genes (DEGs) and potential biomarkers in HD. Results: Our analysis identified 5834 DEGs, including 394 putative druggable genes involved in processes like neuroinflammation, metal ion dysregulation, and blood–brain barrier dysfunction. These genes' expression levels correlated with CAG repeat length, disease onset, and progression. We also identified FTH1 as a promising biomarker for HD, with its expression downregulated in the prefrontal cortex and upregulated in peripheral blood in a CAG repeat-dependent manner. Conclusions: This study highlights the potential of FTH1 as both a biomarker and a therapeutic target for HD. Advanced bioinformatics approaches like RNA-Seq and PSM are crucial for uncovering novel targets in HD, paving the way for better therapeutic interventions and improved clinical trial outcomes. Further validation of FTH1′s role is needed to confirm its utility in HD.

Keywords: Huntington's disease; RNA-Seq; propensity score matching; druggable genes; FTH1; biomarker; neuroinflammation; blood–brain barrier; CAG repeat; transcriptomics

check for updates

Academic Editors: Yujing Li and Yulin Jin

Received: 12 May 2025
Revised: 18 June 2025
Accepted: 24 June 2025
Published: 25 June 2025

Citation: Dias Pinto, J.R.; Faustinoni Neto, B.; Munhoz, L.; Kerkis, I.; Araldi, R.P. From Brain to Blood: Uncovering Potential Therapeutical Targets and Biomarkers for Huntington's Disease Using an Integrative RNA-Seq Analytical Platform (BDASeq®). *Cells* **2025**, *14*, 976. https://doi.org/10.3390/cells14130976

Copyright: © 2025 by the authors. Licensee MDPI, Basel, Switzerland. This article is an open access article distributed under the terms and conditions of the Creative Commons Attribution (CC BY) license (https://creativecommons.org/licenses/by/4.0/).

1. Introduction

Huntington's Disease (HD, OMIM 143100) is a rare and fatal monogenic autosomal-dominant neurodegenerative disorder characterized by progressive motor dysfunction, neuropsychiatric symptoms, and cognitive decline [1,2].

First described in 1872 by George Huntington as a hereditary movement disorder, with a spectrum of choreiform movements, rigidity, cognitive impairments, and behavioral disturbances in families from Long Island (New York, NY, USA) [3,4], the cause of HD was only resolved in 1993, when The Huntington's Disease Collaborative Research Group identified the expansion of cytosine–adenine–guanine (CAG) trinucleotide (>36 CAG repeats) in the first exon of the *HTT* gene (*locus* 4p16.3) as HD's cause [5].

With more than 26,905 published articles since 1903 and 256 clinical trials, with 114 of them evaluating the safety and/or eventual benefits of investigational products in 12,483 enrolled subjects (according to PubMed and Clinical.Trial.gov, respectively—data up to 23 May 2025), the disease remains lacking in treatments capable of modifying its natural history even 153 years since the first report on HD. Approved drugs for HD treatment, tetrabenazine (Xenazine®), deutetrabenazine (Austedo®), and valbenazina (Ingrezza®), only offer benefits for chorea treatment [6–9]. However, by causing postsynaptic depletion of neuroactive monoamines, the use of these drugs is often accompanied by a range of adverse effects (AEs), such as sedation, drowsiness, fatigue, depression, and anxiety, which can hinder daily functioning and exacerbate the already debilitating symptoms of the disease [6,9–15].

Given the absence of disease-modifying therapies, identifying new therapeutic targets is imperative. In this context, RNA sequencing (RNA-Seq) emerges as a powerful tool to uncover druggable genes and biomarkers that could guide drug repositioning efforts or foster novel drug development through computer-aided drug design (CADD) [16,17].

The RNA-Seq workflow begins with RNA extraction from biological samples, followed by either mRNA enrichment or rRNA depletion, as protein-coding RNAs are the primary focus for computer-aided drug design (CADD). The enriched mRNA is then reverse-transcribed into complementary DNA (cDNA), and a cDNA library is constructed. This library is sequenced at a depth of 10–100 million reads per sample using high-throughput platforms, typically from Illumina™. The resulting sequences undergo rigorous quality control assessments, evaluating parameters such as read accuracy (Phred score), exogenous RNA contamination (%GC content), and fragment length distribution. After quality control, reads are aligned to a reference genome to determine the set of expressed genes. Subsequently, mapped reads are quantified, normalized, and statistically compared to controls to identify differentially expressed genes (DEGs) [18,19].

However, the identification of DEGs can be influenced by the theoretical assumptions, normalization strategies, and statistical corrections for multiple comparisons (e.g., *p*-value adjustment or false discovery rate, FDR) employed by different differential expression analysis (DEA) methods [20–22]. Given the lack of a universally accepted gold standard method for DEA, BioDecision Analytics™ developed the Biomarker Discovery Algorithm (BDASeq®) (registered under Brazilian National Institute of Industrial Property number BR512025001097-4) to address these analytical challenges [23,24].

BDASeq® is an integrative analytics-based tool designed to identify putative therapeutic targets (druggable genes) and/or biomarkers of diseases. BDASeq® is divided into three layers: (i) Processing data, which allows the direct uploading of samples from directory or public BioSamples from the Sequence Read Archive (SRA) database using the SRA Toolkit, analyzes sequencing quality control (FastQC [25] and MultiQC [26]), aligns (STAR [27]), and counts the mapped reads (featureCounts [28]), thus generating a counting matrix. (ii) Differential expression, which combines the results of eight different statistical methods that come from the following: (i) Bioinformatics (DESeq2 [22], edgeR [29], limma-Voom [30], NOISeq [31], EBSeq [32], dearseq [33]) and (ii) classical statistics (Wilcoxon [34] and Firth logistic regression [35]). This ensemble of different techniques designed for DEA is performed by the innovative Recursive Method Combination (RMC), which si-

multaneously controls type I and II errors, reducing analytical bias and generating a gene classification list. Finally, there is the (iii) gene target search, which uses Data Analytics and artificial intelligence (AI) algorithms to identify potential druggable genes and/or biomarkers, as schematically illustrated in Figure 1. In addition, BDASeq® also counts on the optional control sample selection tool. Using the Propensity Score Matching (PSM) algorithm [36,37], a quasi-experimental method introduced by Rosenbaum and Rubin [36], BDASeq® reduces case–control selection bias, increasing target gene accuracy identification for CADD [18,24,38]. Additionally, the use of an unsupervised algorithm devoted to identifying outliers through clustering approaches was employed to remove undesired samples from the expression matrix.

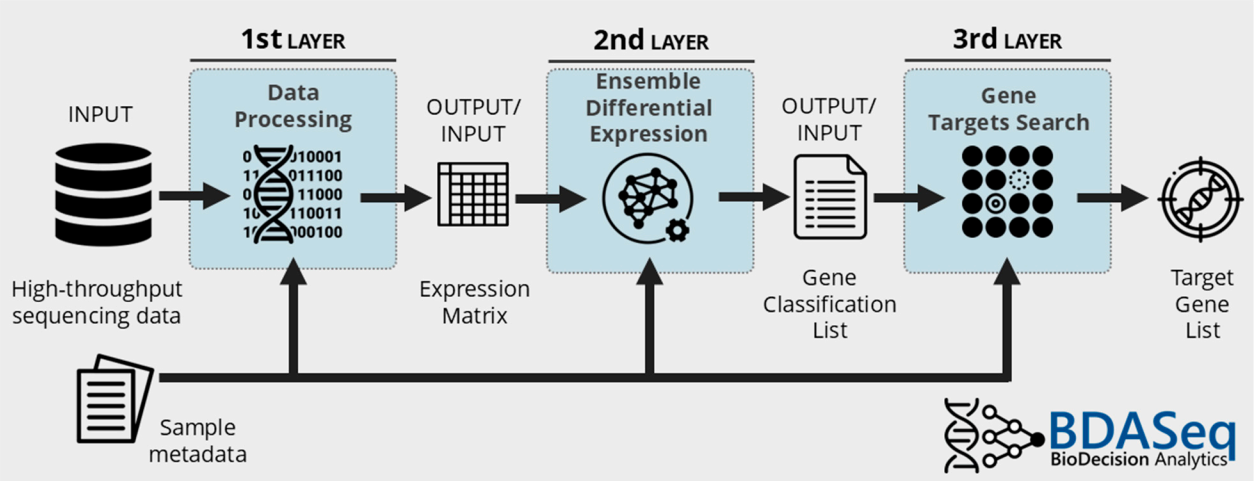

Figure 1. Schematic model of the BDASeq® tool. High-throughput sequencing files/data (FASTQ) are imported into the tool using the SRA Toolkit. To minimize case–control bias, control samples are selected using the Propensity Score Matching (PSM) algorithm. Pre-selected BioSamples from controls and cases are then subjected to quality control analysis using FastQC. Samples that pass quality control are aligned to a reference genome using the STAR aligner and mapped reads are quantified using the featureCounts, generating a count matrix that serves as the input to the next step—differential expression analysis. In the differential expression analysis phase, eight different methods (DESeq2, edgeR, limma-Voom, NOISeq, EBSeq, dearseq, Wilcoxon, and Firth logistic regression) are applied individually. Results are then combined using the disruptive Recursive Method Combination (RMC) algorithm, which simultaneously reduces type I and type II errors, thus minimizing analytical bias. The process also filters out undesired samples through outlier-detection techniques. Following this integrative analysis, genes are classified into six categories: zero-count genes (ZCGs), low-count genes (LCGs), equally expressed genes (EEGs), non-relevant genes (NRGs), up- (URGs) or downregulated genes (DRGs). Finally, in the target gene search layer, artificial intelligence (AI) algorithms are employed to both identify putative target as well as retrieve URGs and DRGs associated with clinical–pathological features of interest (based on the sample metadata variables). BDASeq® is proprietary intellectual property of BioDecision Analytics Ltd., registered in Brazilian National Institute of Industrial Property (INPI, Rio de Janeiro, Brazil, BR512025001097-4).

This large-scale transcriptomic analysis, which included the reanalysis of C from 12 independent BioProjects available in the SRA database, represents the most comprehensive RNA-Seq-based study of HD to date. Supported by the International Huntington Association (IHA), Brazil Huntington Association (ABH), and the Brazilian Huntington Union House (CBUA), our findings uncovered 394 novel putative druggable genes and 18 potential blood biomarkers linked to clinical–pathological features of HD, including FHT1. These discoveries pave the way for new therapeutic strategies and provide crucial tools for monitoring disease progression and therapeutic responses in future clinical trials.

2. Materials and Methods

2.1. Ethical Approval

This study utilized sequencing data from individuals who tested positive for the HD gene and neurologically normal individuals in the SRA public database. Formal ethical approval was not required, as the identities of all participants remain anonymous according to SRA ethical guidelines. No additional institutional review board (IRB) approval was necessary.

2.2. BioProject (Data) Description

There were a total of 778 brain BioSamples (n = 778) from 12 independent BioProjects (PRJNA271929, PRJNA316625, PRJNA670925, PRJEB59710, PRJNA253002, PRJNA557205, PRJNA602538, PRJNA531456, PRJNA398545, PRJNA729761, PRJNA388174, and PRJNA755746) containing transcriptomic data (FASTQ files) from the prefrontal (Broadman's area 9) and motor cortex (Broadman's area 4); 233 blood BioSamples (n = 233) from three independent BioProjects (PRJNA225101, PRJNA559372, and PRJNA261011) of potential cases and controls were identified in the SRA database as potential data for the analysis, as illustrated in Figure 2. The study considered eligible BioSamples from humans carrying the *mHTT* gene (cases), as confirmed by genetic diagnostics (declared in BioProject metadata, cases), or those not carrying the *mHTT* gene whose cause of death was unrelated to any neurodegenerative disorder (controls). To avoid case–control bias, control samples without age matching with cases were excluded using the MatchIt package in R [39], as implemented into the BDASeq® platform (Propensity Score Matching (PSM) algorithm). Only samples passing basic quality control measures, such as RNA integrity and sequencing depth thresholds, were included for further analysis.

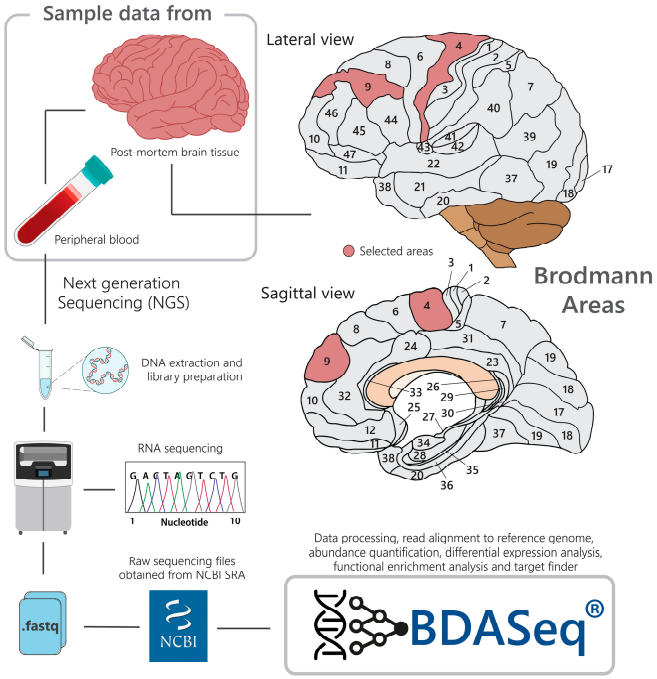

Figure 2. Schematic illustration of the study design. Eligible brain (Broadmann areas (BAs) 4 and 9) and blood BioSamples (FASTQ files) from HD-positive (cases) and neurologically normal controls were downloaded from the SRA database (implemented into BDASeq®). Using BDASeq®, FASTQ files are processed, being submitted to quality control analysis, sequence alignment/mapping, and read counts. Next, read counts are subjected to differential expression analysis using the RMC algorithm. Differentially expressed genes are combined with clinical–pathological features to identify potential therapeutic targets or biomarkers using AI.

2.3. Control Sample Selection by Age Distribution

In a previous study, we showed that the use of older controls indeed leads to the misidentification of DEGs, negatively affecting the discovery of druggable genes and/or biomarkers. This finding highlights the critical importance of considering the age of control samples in RNA-Seq analysis and suggests that age matching should be included as the best practice for such investigations [18]. Therefore, using the MatchIt package in R [39], implemented in the BDASeq® platform, we created a virtual group of pre-eligible BioSamples from neurologically normal individuals, age-matched to HD gene-positive individuals at a 1:1 ratio (HD gene-positive subject: neurologically normal subject). To validate the outcomes of the control sample selection, we visually assessed the age distribution before and after PSM through both boxplot and density plot. Additionally, statistical confirmation of the quality of age distribution was carried out using Student's *t*-test (p-value > 0.05), all executed within the R environment (version 4.4.1, available on https://www.r-project.org/). A p-value greater than 0.05 was considered indicative of no significant difference between groups after matching.

2.4. Data Processing, Differential Expression Analysis, and Target Discovery Using BDASeq®

FASTQ files of eligible BioSamples, including age-matched control samples, were downloaded from the SRA database using SRA Toolkit. Pre-eligible BioSamples were subjected to quality control analysis using FastQC [25] and MultiQC [26]. Samples selected for this study met the following criteria: a Phred score above 30, fragment length of 100–150 bp, and %GC of 50% ± 4, according to the recommendations by Conesa et al. [40].

Eligible BioSamples were then aligned with the human reference genome GRCh38 (release 108) using STAR [27]. Mapped reads were counted with featureCounts [28]. This process resulted in a count matrix, which serves as input for the next step differential expression analysis (DEA). Due to the combination of different studies, with different strategies, the batch effects from the raw count matrix were removed by using the ComBatSeq algorithm [41]. Bioinformatic tools used for data downloading and processing are implemented in the first layer of BDASeq® (data processing). Outliers samples were filtered out using the combination of unsupervised algorithm with clustering analysis. DEGs analysis was performed using eight different methods: DESeq2 [22], edgeR [29], limma-Voom [30], NOISeq [31], EBSeq [32], dearseq [33], Wilcoxon [34], and Firth logistic regression [35]. Results from these methods are integrated using the Recursive Method Combination (RMC) algorithm to minimize analytical bias. Genes were then classified as zero (ZCGs), low (LCGs), equally expressed (EEGs), non-relevant (NRGs), up- (UGRs) or downregulated genes (DRGs), as previously proposed by us [18]. The criteria of classification used are summarized in Table 1. Bioinformatic and statistics tools used for DEA and the RMC algorithm are part of the second layer of BDASeq® (differential expression). Subsequently, the most relevant genes (UGRs and DRGs) and their association with clinical features of Huntington's Disease (HD)—including CAG repeat number, age at onset, Vonsattel grade (indicative of brain degeneration), and lifespan—were identified using supervised classification algorithms coupled with feature selection techniques [41]. This feature selection step, combined with feature (i.e., gene) importance measurements, were integrated into the third layer of BDASeq® (Gene Target Search). Results were summarized in tables, heatmaps, and boxplots based on normalized read counts.

Table 1. Gene classification criteria used by BDASeq®.

Classification	Criteria
Zero-count genes (ZCGs)	Genes with row counts = 0
Low-count genes (LCGs)	Genes with normalized counts < 10
Equally expressed genes (EEGs)	Genes with no statistical differences between cases and controls, adjusted *p*-value (FRD [1]) > 0.05)
Non-relevant genes (NRGs)	Genes with adjusted *p*-value (FRD) < 0.05, but |log2FC| < 0.40
Downregulated genes (DRGs)	Genes with adjusted *p*-value < 0.05 and log2FC < −0.40
Upregulated genes (URGs)	Genes with adjusted *p*-value < 0.05 and log2FC < 0.40

[1] FDR—false discovery rate.

3. Results

3.1. Study Design and Sample Selection

From the 778 BioSamples (n = 778) across 12 independent BioProjects (File S1) containing transcriptomic data from the prefrontal cortex of HD gene-positive (cases) or neurologically normal individuals (controls), 425 BioSamples (n = 425) were excluded for not meeting eligibility criteria. Specifically, the following criteria were used for exclusion: (i) non-human samples (n = 50), (ii) non-HD samples (n = 226), (iii) samples from non-prefrontal cortex tissue (n = 71), (iv) samples failing quality control (n = 55), (v) juvenile control samples (n = 20), and (vi) asymptomatic FD cases (n = 3). After this exclusion, 353 BioSamples (n = 353) were deemed eligible, comprising 146 gene-positive cases and 207 neurologically normal controls (Figure A1).

To minimize case–control bias, the BDASeq® tool employed a PMS algorithm to select the age-matched subset of control samples (age-matched controls, n = 146, 59.1 ± 12.3 years) comparable to the HD group (n = 146, 57.9 ± 14.4 years) Consequently, 61 unmatched control samples (80.8 ± 14.4 years) were excluded (Figure 3). In total, 296 prefrontal cortex samples were included in the final analysis: 146 from HD gene-positive cases and 146 matched controls. To our knowledge, this constitutes the largest transcriptomic study of HD compiled into data, as recognized during the MENA Congress for Rare Disease 2024 [24,38] and by the FAPESP Agency (https://agencia.fapesp.br/a-startup-supported-by-fapesp-is-conducting-one-of-the-largest-studies-on-huntingtons-disease/51647, accessed on 23 June 2025).

3.2. Aging Promotes Transcriptional Alterations in the Prefrontal Cortex

As anticipated, a statistically significant difference was observed between HD cases and controls (Figure A3). Reanalysis of one of the 12 BioProjects (PRJNA271929) revealed that using control samples without proper age matching with cases increases both type I and II errors, leading to misidentification of DEGs [18].

Dimensionality reduction analysis using Uniform Manifold Approximation and Projection (UMAP) of the transcriptomic profiles from the 353 BioSamples analyzed in this study showed that cases and controls were distinct in the multidimensional space (Figure A3A), confirming that HD induces transcriptional changes in the prefrontal and motor cortex, as expected. However, clustering analysis revealed that 353 BioSamples are grouped in three clusters (Figure A3B): C0 and C1, predominantly composed of neurologically normal controls, and C2, primarily comprising HD gene-positive individuals (Figure A3C). Further analysis of the control groups revealed that cluster C0 consisted of neurologically normal

controls who were older than those in cluster C1, as demonstrated in Figure A3D. These findings confirm that aging contributes to transcriptional changes in the prefrontal cortex and emphasizes the importance of carefully selecting control samples to prevent target misidentifications, as we previously reported [18]. Using clustering techniques, it was possible to identify and remove 20 samples considered as outliers capable of drastically affecting the differential expression analysis (depicted as C-1 cluster in Figure A3B). The exclusion of these 20 samples were based on the combination of 2D UMAP representation of the bulk gene expression (removing zero- and low-count genes) with DBSCAN analysis. DBSCAN, in nature, works by defining clusters as densely packed regions separated by regions of lower density. This approach allows DBSCAN to discover and label sparse distributed samples as noise, i.e., outliers.

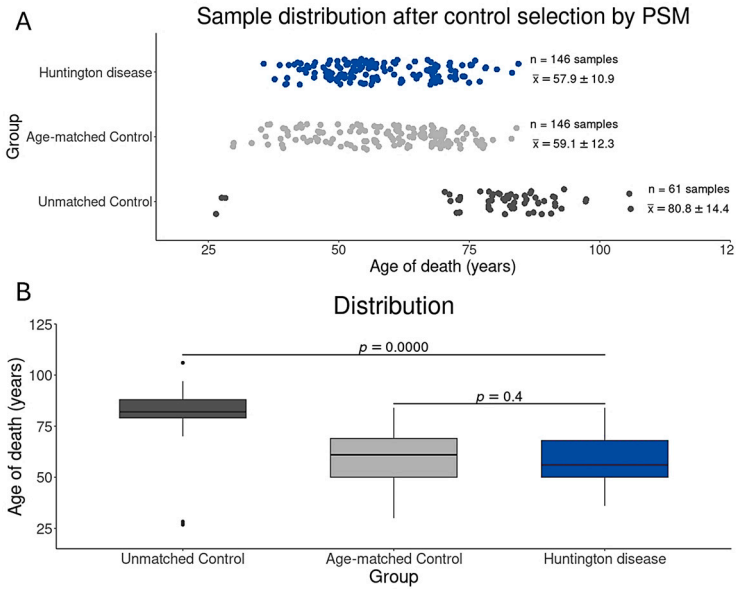

Figure 3. Age distribution after PSM-based sample selection (**A**). Note that the PSM appropriately selects 146 control samples with age distribution (age-matched controls, 59.1 ± 12.3 years) statistically similar to cases (Huntington disease, 57.9 ± 10.9 years) (**B**), excluding 61 unmatched control samples from older neurologically normal individuals (80.8 ± 14.4 years). Statistical analysis was performed using one-way ANOVA, followed by the Tukey post hoc test, both with significance levels of 5%.

3.3. BDASeq® Identified 394 Potential Druggable Targets for HD

Transcriptomes from the cases and controls were compared by using the BDASeq®. Of the 62,703 transcripts annotated in the human reference genome, 4005 transcripts were classified as ZCGs, and 32,533 were classified as LCGs—both categories corresponding genes that are not expressed by the prefrontal and motor cortex. Among the expressed genes (normalized counts > 10), 12,901 transcripts were categorized as EEGs, and thus were excluded as potential therapeutic targets for HD. A total of 7430 transcripts were identified as NRGs, being statistically significant by adjusted *p*-value (FDR) but lacking a meaningful log2FC, and were therefore considered suboptimal for drug development (criteria of NRG definition available on Table 1). Conversely, BDASeq® identified 5834 DEGs, comprising 3729 as URG and 2105 as DRG transcripts (Figure 4, File S2).

Of these 5834 DEGs, 2896 encode proteins—representing 49.64% of total the DEGs—and were considered potential druggable targets (File S2). Among these protein-coding DEGs, 83.53% (2057/2377) were concordantly identified by both BDASeq® and the traditional DESeq2 pipeline (Figure 5A, File S2). However, BDASeq® uniquely identified 839 additional protein-coding targets not detected by DESeq2—putative false negative DEGs—while DESeq2 identified 320 targets not captured by BDASeq®—putative false

positive (Figure 5A, File S2). These discrepancies are consistent with expectations as the integration of the PSM and RMC within BDASeq® is designed to simultaneously control type I and type II errors, thereby refining gene classification, as illustrated in the Sankey diagram (Figure 5B).

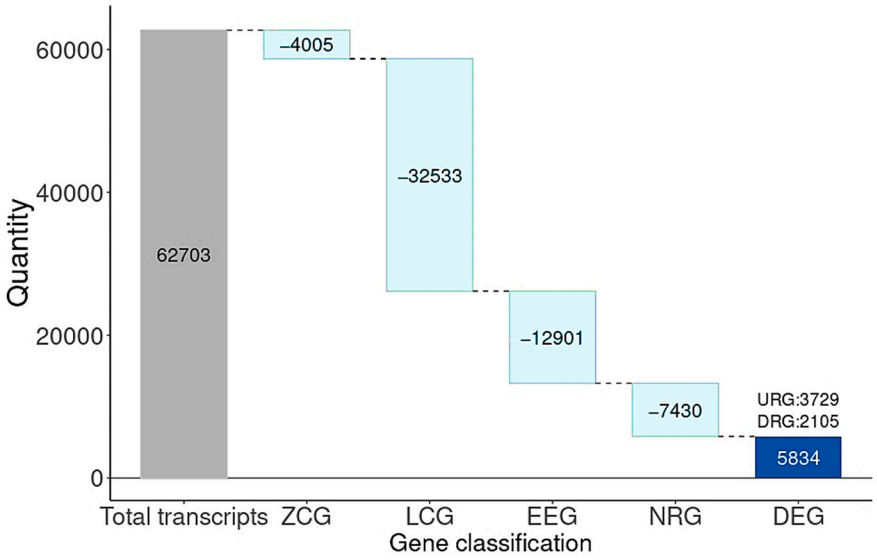

Figure 4. Waterfall plot showing the total number of differentially expressed genes identified in the prefrontal and motor cortex of HD gene-positive individuals in relation to the controls. Note that, from the 62,703 transcripts encoded by the human reference genome, 36,538 (4005 ZCGs and 32,533 LCGs) transcripts are not expressed by the selected brain areas. Fron the expressed genes, 12,901 are equally expressed by cases and controls (EEGs); 7430 transcripts show a statistically significant adjusted *p*-value (FDR), but with no significant log2FC (NGR); and 5834 transcripts are differentially expressed between cases and control. Of these, 3729 are upregulated (URG), and 2105 are downregulated (DRG).

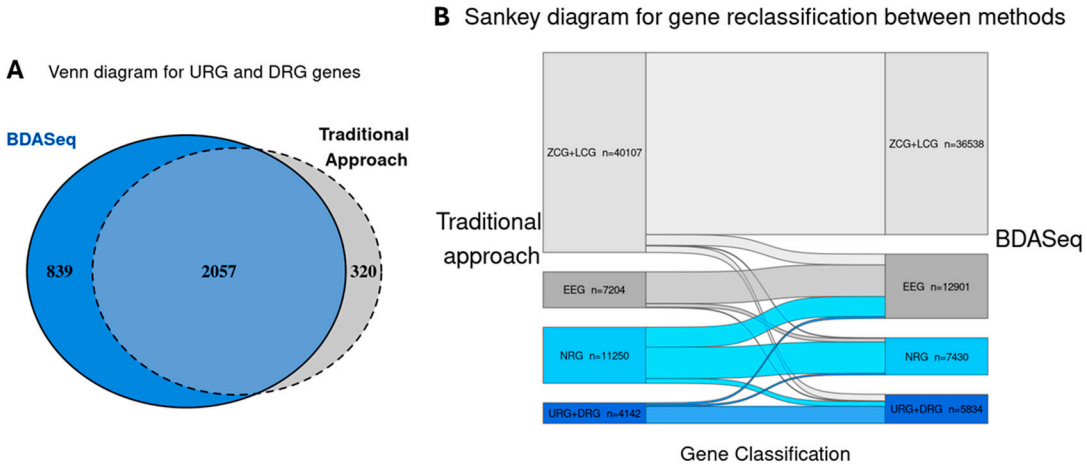

Figure 5. Comparative analysis between BDASeq® and the traditional approach using DESeq2 and the commonly used log2FC criteria for target selection. Venn diagram comparing the protein-coding genes (potential drug targets and/or biomarkers) identified by BDASeq and the traditional approach. Results show that BDASeq® identified 2057 URGs and DRGs in common with the traditional approach but identified 839 potential targets not identified by the traditional approach. Besides this, BDASeq® excludes 320 potential targets identified by the traditional approach (putative false positive targets) (**A**). The Sankey diagram shows that by appropriately selecting age-matched control samples with cases and combining eight different DEA techniques using the innovative RMC algorithm, BDASeq® reclassifies the gene status of the traditional approach (**B**).

Traditionally, DEGs are ranked solely by their log2FC, optionally combined with FRD-adjusted *p*-values (FDR), to shortlist the most significantly up- or downregulated genes for further consideration as drug targets or biomarkers [42]. However, as previously discussed [18], this approach can result in target misclassification. To address this limitation, BDASeq® incorporates an AI-driven feature selection algorithm that prioritizes candidate genes based on their expression distribution between cases and controls rather than fold-change magnitude alone. Using this algorithm, BDASeq® counts on a feature selection AI-based algorithm that appropriately selects target genes based on their distribution between cases and controls. Using this algorithm, BDASeq® identified 394 protein-coding genes as druggable targets and/or biomarkers for HD (Figure 6, File S3).

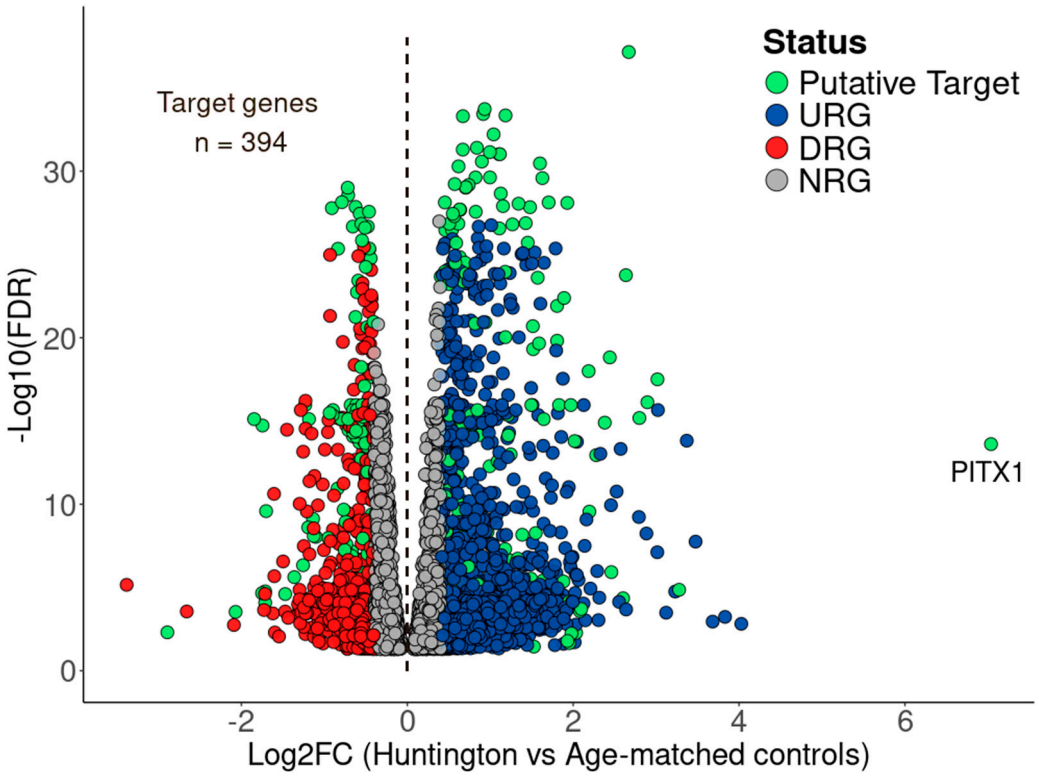

Figure 6. Volcano plot showing the downregulated (DRG, in red) and upregulated (URG, in blue) identified by the RMC algorithm, as well as the putative target protein-coding genes (394) identified in prefrontal and motor cortex of HD-positive individuals using the AI-based feature selection algorithm from these DRGs and URGs.

Comparative analysis of normalized expression values between HD and control samples showed that 210 of these genes were upregulated, and 184 were downregulated in the prefrontal cortex and motor cortex of HD gene-positive individuals (Figure 7, File S3). Furthermore, the Gini coefficient—a measure of statistical dispersion reflecting intergroup expression variability—ranged from 0.3 (*ANKRD62*) to 1.0 (*PITX1*), supporting the robustness of the gene selection process (File S3).

Notably, when comparing BDASeq® results to those from DESeq2, only 103 of the 394 genes (26.14%) were identified by both approaches (Figure A4). This indicates that BDASeq®'s AI algorithm revealed 291 novel targets that would have been overlooked using conventional log2FC-based ranking (Figure A4), highlighting its potential to uncover new avenues for drug development, repositioning, and prognostic biomarker discovery in HD.

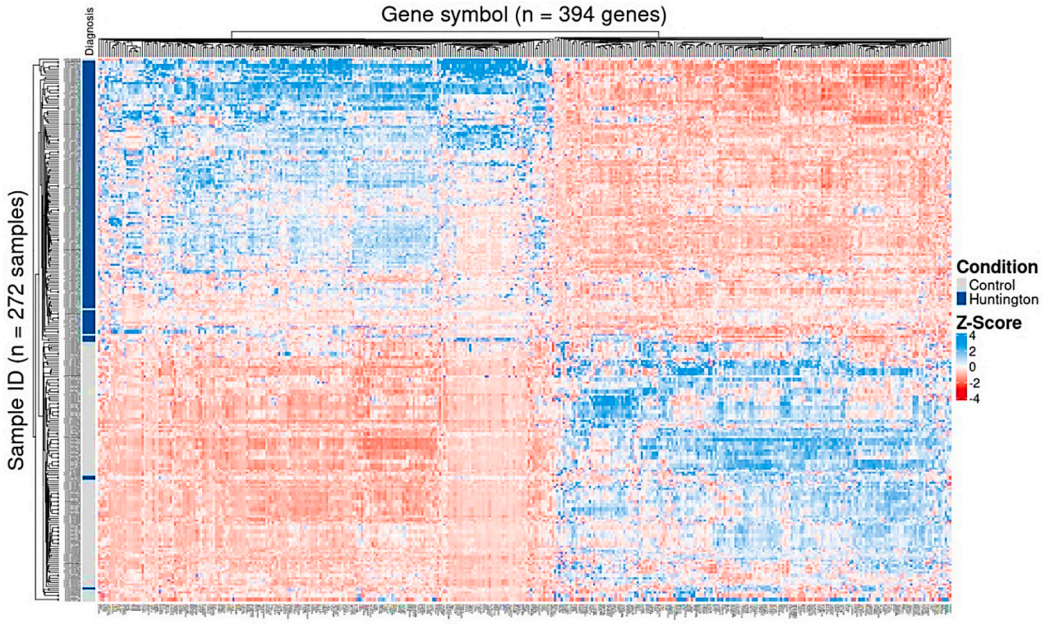

Figure 7. Heatmap showing the normalized counts from the 394 protein-coding genes potentially identified as targets by BDASeq®. Results confirm that these genes are differentially expressed in prefrontal and motor cortex from HD-positive individuals when compared to the prefrontal cortex of neurologically normal controls.

3.4. Putative Druggable Genes Identified by BDASeq® Are Associated with Dysregulated Biological Processes in HD

Given that a druggable gene is ideally defined as a protein-coding gene linked to a disease-specific biological process that can be therapeutically modulated by a drug [43], the 394 protein-coding genes identified by BDASeq® were subjected to functional enrichment analysis using multiple Gene Ontology (GO) databases. The enrichment results revealed that these candidate genes are significantly involved in biological processes and molecular functions known to be disrupted in HD. These include responses to metal ions, cholesterol metabolism, neuroinflammation, transport across the blood–brain barrier, negative regulation of the cell cycle, disruption of membrane scaffolding, axon guidance, and neurotransmission (Figure 8, Table 2, File S4). These findings reinforce the biological relevance of the BDASeq®-identified targets, as they are functionally tied to core pathological mechanisms of HD and may thus serve as promising candidates for therapeutic development or repositioning.

Table 2. Target genes involved in HD-related pathophysiological process.

Process	Target Genes Identified	Pathophysiological Process	Reference
Metal ion response	*CDH1, MMP9, MT1, MTIF, MT1G, MTIH, MT1M, MT1X, MT2A*	- Copper, manganese, and zinc are increased in CSF in early HD - Copper and iron are increased in striatum of HD, causing pro-oxidant effects and neurodegeneration - Copper and zinc increased mHTT aggregation	Pfalzer et al. [44] Fox et al. [45] Rosas et al. [46] Cordeiro et al. [47]

Table 2. *Cont.*

Process	Target Genes Identified	Pathophysiological Process	Reference
Cholesterol metabolism	*CD36, DHCR24, FASN, HMGCS1, MVD, TM7SF2*	- Cholesterol is an essential membrane component in the CNS - Cholesterol cannot cross the blood–brain barrier (BBB) due to its association with lipoproteins, so it is synthesized locally in the CNS - HTT protein is a key regulator of lipid metabolism - plasma 24S-hydroxycholesterol is reduced in HD patients proportionally to disease progression - mHTT decreases the maturation of SREBP and the upregulation of LXR and LXR-targeted genes (SREBP, ABCG1, and ABCG4, HMGCoA reductase, ApoE), resulting into a lower synthesis and transport of cholesterol from astrocytes to neurons via ApoE - HD attenuates brain sterol synthesis and accumulation of cholesterol in neuronal membranes, leading to neuronal loss	Kacher et al. [48] Leoni et al. [49] Karasinka et al. [50]
Neuronflammation	*ADCY1, CAMKK2, CHRNB2, PB41L3, KCNA1, KCNC3, KCNC3 KCNJ12, NRG1, NRXN3, PPIA4, PRKKCG, SYT2*	- mHTT causes inflammatory responses in both CNS and peripheral tissues - increase in multiple cytokines in the plasma (IL-1β, IL-4, IL-6, IL-8, TNF-α, IL-10) and striatum (IL-6, IL-8 and TNF-α) of HD patients - Patients with HD have significantly lower plasma concentrations of IL-4, a marker of responses from T-helper-2 cells, than healthy control	Jia et al. [51] Björkqvist et al. [52] Silvestrini et al. [53] Du et al. [54] Ellrichmann et al. [55] Björkqvist et al. [52]
Transport across the brain-blood barrier	*ABCC4, ANXA3, BTG1, ITGB8, SFRP2, SIRT1, SLC16A12, SLC22A2, SLC22A8, SLC38A2, SLC5A3, SCL7A2, TWIST1*	- mHTT expression alters the neurovasculature by increasing cerebral blood volume, small vessel density, and BBB permeability in rodent models of HD and patient tissue	Katt et al. [56] Knox et al. [57] Hua et al. [58] Lin et al. [59] Vignone et al. [60] Pardo et al. [61] Yaun et al. [62]
Axon guidance	*AZIN2, CHRNB2, CNTN6, DCTN1, DPYSL5, EPHA10, HTR2C, KCNA1, KCNA3, MAP1B, NEFH, PARD3, PARD6B, POU4F1, PRKCG, RGS11, RIT2, ROCK1, SCN1B, SDC2, SEMA4D, SEMA5B, SGK1, SLC30A3, SLC39A12, SYT2*	- mHTT causes developmental defects affecting axon growth - mHTT causes axon growth dysfunctions	Capizzi et al. [63] Li et al. [64]

Table 2. *Cont.*

Process	Target Genes Identified	Pathophysiological Process	Reference
Neurotransmission	*ATP2B2, ATP2C2, ATP6V0E2, ACNA1H, CALHM1, CHRNB2, DHCR24, GPLD1, KCNA1, KCNC3, KCNS2, MECR, NRG1, OTOF, P2RX2, P2RX6, PLA2G4C, PLBD2, PNPLA3, RIT2, SCN1B, SCN4B, SEMA4D, SEMA5B, SLC30A3, SMPD3, SV2C, SYT2, TM7SF2, TMEM163, TRPM1, VAMP1*	- neurotransmission is altered in HD, mainly GABAergic neurotransmission	Garret et al. [65] Bruyin [66]

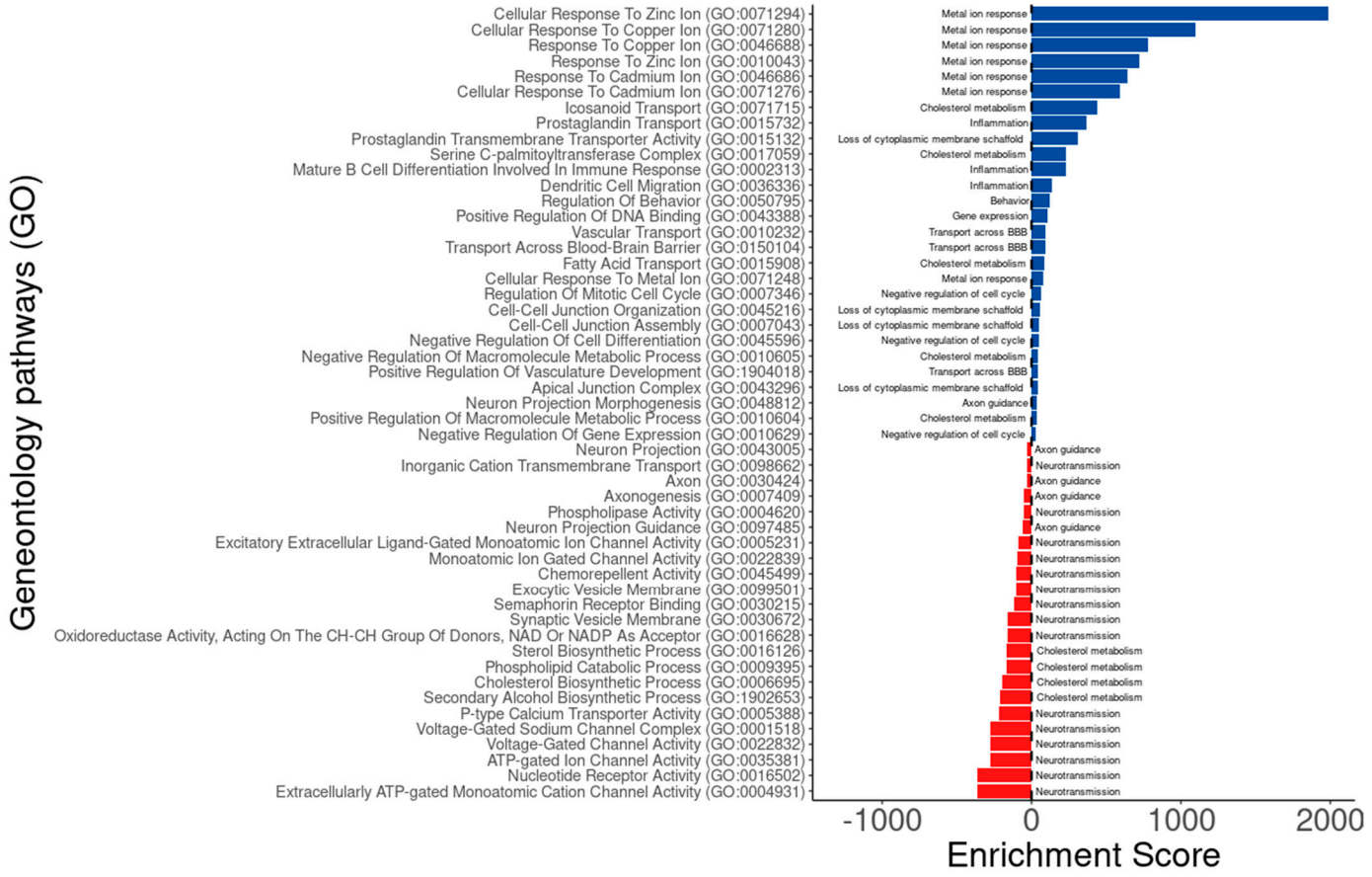

Figure 8. Functional enrichment analysis per overrepresentation (ORA) of the 394 target genes identified by BDASeq®. Results show that the target genes positive (in blue) and negative (in red) regulate biological pathways involved in HD pathophysiology, being related to metal ion response, inflammation, behavior, negative regulation of the cell cycle, transport across the brain–blood barrier (BBB), loss of membrane scaffold, axon guidance, neurotransmission, and cholesterol metabolism. Results obtained in terms of Gene Ontology (GO), using the Erichr webservice.

3.5. Target Genes Identified by BDASeq Are Involved in Aging-Related Processes Exacerbated in HD

Supporting previous evidence that HD exacerbates aging-related biological processes [67–69]; analysis revealed that 149 out of the 394 BDASeq-identified target genes (37.81%) are associated with aging signatures across multiple tissues, including the brain (Figure A5, File S4). These findings provide a molecular basis for the systemic clinical manifestations of HD beyond neurodegeneration. In addition to brain dysfunction, HD is known to cause: (i) skeletal muscle impairments, associated with chloride and potassium channel dysfunction, resulting in muscle hyperexcitability, hypertonicity, twitching, and atrophy [70–73]; (ii) ocular alterations, including retinal nerve fiber layer thinning [74–78]; (iii) bone marrow disruption; (iv) immune system dysregulation, leading to platelet abnormalities [76] and increased production of pro-inflammatory cytokines [79]. Altogether, the 149 aging-associated target genes identified by BDASeq® offer promising opportunities for the development of therapeutic strategies that address both the neurological and systemic features of HD.

3.6. Target Genes Identified by BDASeq Are Deregulated in Brain Regions Affected by HD

Analysis revealed that 391 out of the 394 BDASeq-identified target genes (99.23%) are expressed in brain regions known to be progressively affected in HD, including the cingulate cortex, striatum, caudate nucleus, thalamus, motor cortex, substantia nigra, and cerebellum (Figure A6, File S4). As expected, the majority of these 391 are expressed in brain regions most vulnerable to HD pathology, such as the striatum [70,71], cingulate [72,73], and prefrontal cortex [74–76] (Figure A6, File S4). This observation aligns with the known neuroanatomical progression of HD, as the prefrontal cortex maintains strong functional connectivity with both the cingulate cortex [77] and striatum [78], which may explain the overlapping gene expression profiles observed. These findings reinforce the relevance of the identified targets, as they are localized to key regions implicated in HD pathophysiology and may contribute to region-specific neurodegeneration.

3.7. BDASeq® Identified CAG- and Onset-Age-Related Target Genes

Statistical analysis revealed a strong and significant negative correlation between the CAG repeat length and onset age (p-value = 0.0000 and R = 0.8160, Figure 9A) as well as between CAG repeat length and death age (p-value = 0.0000 and R = 0.8538, Figure 9B). Conversely, a significant positive correlation was observed between age at onset and age at death (p-value = 0.0000 and R = 0.9132, Figure 9C).

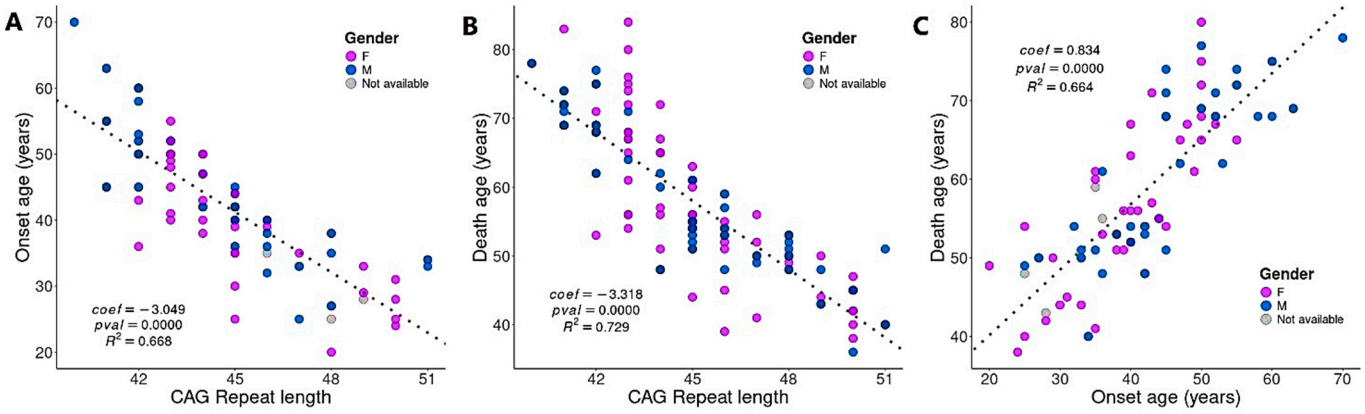

Figure 9. Relevant clinical–pathological features identified using the BDASeq®. Results show a negative correlation between the CAG repeat length and the onset (**A**) and death age (**B**), as well as a positive correlation between the onset and death age (**C**). Doted line describe linear regression.

Given that the CAG repeat length is critical clinical–pathological hallmark of HD closely associated with both disease onset and progression, we applied the BDASeq® AI algorithm to further interrogate the 394 previously identified protein-coding genes (considered potential druggable targets and/or biomarkers for HD). This analysis identified five DRGs and seven URGs whose expression levels are significantly associated with CAG repeat length, highlighting their potential as CAG-related target genes (Table 3, Figure 10). Functional enrichment analysis of these genes revealed relevant biological processes, notably involving DHDDS, a gene implicated in glycosylation and neurodegenerative disease mechanisms.

Table 3. Genes identified by the BDASeq AI algorithm as CAG-repeat length-related targets.

Gene	Classification	*p*-Value	Log2FC	FDR	Pathways [1]
TRMT9B	DRG	0.0388	−0.5504	0.0001	0
SPINK8	DRG	0.0480	1.1801	0.0000	1
GCNT4	DRG	0.0388	−0.4312	0.0004	0
DYDC2	DRG	0.0321	−0.8206	0.0003	0
TNIP3	DRG	0.0264	−1.7133	0.0000	0
FAM83H	URG	0.0189	−0.5040	0.0001	0
RNF123	URG	0.0216	−0.4283	0.0000	0
SPON2	URG	0.0099	−0.8406	0.0000	0
ZSCAN1	URG	0.0215	−0.7667	0.0000	0
GLB1L2	URG	0.0264	−0.5157	0.0000	1
TMEM236	URG	0.0123	1.5482	0.0000	0
DHDDS	URG	0.0263	−0.4200	0.0000	23

[1] Number of pathways in which each gene is involved.

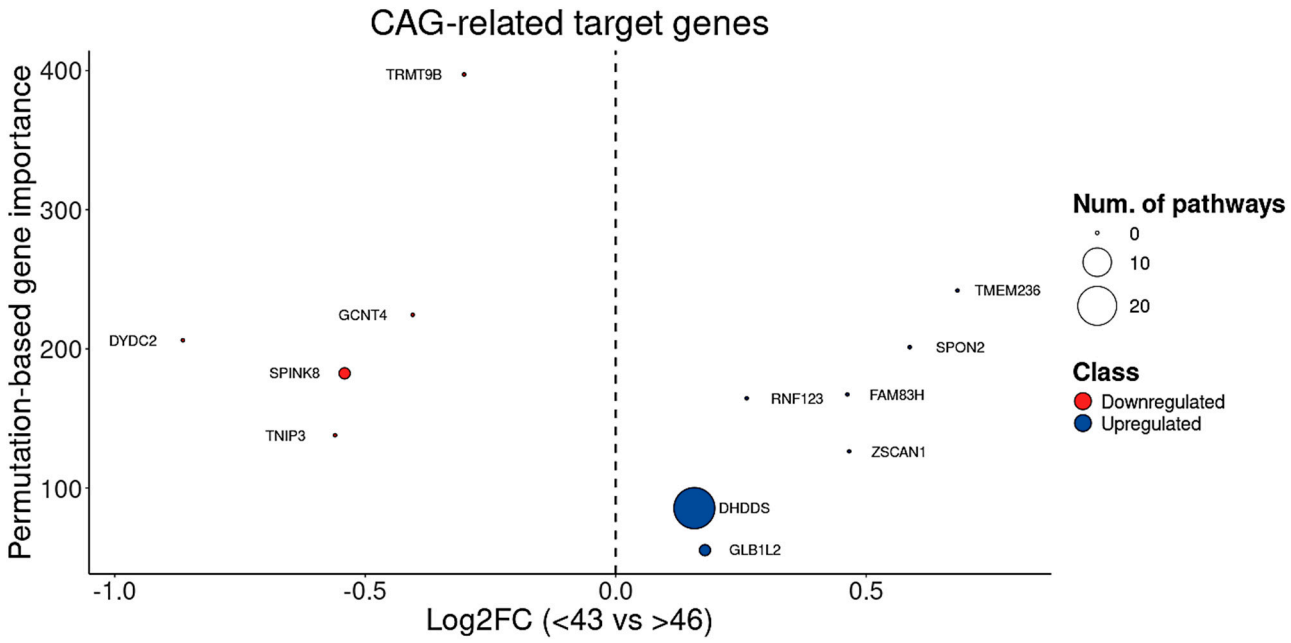

Figure 10. Analysis of the 12 CAG-related target genes showing that, from these genes, five are downregulated and seven are upregulated. Circle diameter indicates the number of pathways in which each gene is involved. The comparison is made considering both superior and inferior extremes of CAG distribution across HD-positive cases.

Moreover, considering the tight relationship between CAG repeat length and disease onset (Figure 9A), and the positive correlation between onset and age at death (Figure 9B,C),

the BDASeq® AI algorithm was also used to identify onset age–related target genes. This analysis yielded 59 potential druggable genes and/or biomarkers, including 33 DRGs and 26 URGs whose expression levels significantly correlate with age at onset (Table 4, Figure 11).

Table 4. Genes identified by the BDASeq AI algorithm as onset age-related targets.

Gene	Classification	*p*-Value	Log2FC	FDR	Pathways [1]
OR3A2	DRG	0.0292	−0.5151	0.0064	0
PRCD	DRG	0.0007	−0.4182	0.0025	0
CD177	DRG	0.0092	1.9313	0.0162	0
VWA7	DRG	0.0216	−0.7744	0.0001	0
PDZD7	DRG	0.0052	−0.5045	0.0000	1
NRBP2	DRG	0.0415	−0.4667	0.0000	0
EPHA10	DRG	0.0178	−0.6829	0.0000	2
SCN4B	DRG	0.0439	−0.5889	0.0000	22
CIDEA	DRG	0.0086	−0.6417	0.0004	1
PLEKHD1	DRG	0.0006	−0.7914	0.0001	0
CES4A	DRG	0.0292	−0.6246	0.0000	1
FASN	DRG	0.0464	−0.4322	0.0000	2
FTH1	DRG	0.0392	−0.5208	0.0000	0
CORO6	DRG	0.0099	−0.4891	0.0000	0
MVD	DRG	0.0027	−0.5133	0.0004	5
MAMDC2	DRG	0.0042	0.5831	0.0004	0
MTHFD2L	DRG	0.0121	0.4417	0.0002	0
TRIM17	DRG	0.0292	−0.4646	0.0000	0
NRG1	DRG	0.0121	−0.6523	0.0000	2
CEP112	DRG	0.0403	0.5611	0.0000	0
SYT2	DRG	0.0049	−1.7452	0.0000	37
STAC2	DRG	0.0002	−0.5169	0.0000	6
CBLN3	DRG	0.0049	−1.7130	0.0001	0
VAMP1	DRG	0.0002	−0.6175	0.0000	25
TP53TG5	DRG	0.0464	−0.7439	0.0000	0
WNT3	DRG	0.0086	0.5000	0.0001	21
SCN1B	DRG	0.0027	−0.5948	0.0000	56
PLA2G4C	DRG	0.0025	−0.4849	0.0000	3
SEC14L5	DRG	0.0167	−0.5010	0.0000	0
P2RX6	DRG	0.0086	−0.5360	0.0000	13
MYO15A	DRG	0.0001	−0.5266	0.0000	6
RGS11	DRG	0.0080	−0.4597	0.0001	1
TNIP3	DRG	0.0074	−1.7133	0.0000	0
MRC1	URG	0.0464	1.8902	0.0000	4
STUM	URG	0.0229	−0.8045	0.0000	0
KCNJ12	URG	0.0392	−0.5354	0.0001	8
TMEM151B	URG	0.0244	−0.4485	0.0000	0
FAM91A1	URG	0.0167	0.4735	0.0000	2
TCP11L1	URG	0.0147	−0.4481	0.0000	1
PDGFD	URG	0.0427	1.0627	0.0007	9

Table 4. *Cont.*

Gene	Classification	*p*-Value	Log2FC	FDR	Pathways [1]
SHOX2	URG	0.0006	2.6702	0.0000	16
ABCA1	URG	0.0370	0.9330	0.0000	16
CA10	URG	0.0019	−0.6081	0.0000	0
SPHKAP	URG	0.0275	−0.9092	0.0000	0
SRD5A1	URG	0.0329	−0.4246	0.0000	1
ARPP19	URG	0.0329	−0.4803	0.0000	1
FEZF1	URG	0.0002	1.6361	0.0000	6
SIX1	URG	0.0310	1.9791	0.0058	5
TWIST1	URG	0.0027	1.0096	0.0009	68
SLC9A2	URG	0.0229	0.6608	0.0007	0
GABRR2	URG	0.0339	1.3858	0.0000	1
SMPD3	URG	0.0121	−0.4803	0.0000	6
TBX5	URG	0.0109	2.0175	0.0000	37
PPEF1	URG	0.0001	−1.1849	0.0000	0
TMEM38A	URG	0.0349	−0.5346	0.0000	7
ARHGAP10	URG	0.0010	0.6159	0.0000	4
PITX1	URG	0.0025	7.0377	0.0000	19
RCN1	URG	0.0023	0.6193	0.0000	4
NRXN3	URG	0.0392	−0.5461	0.0000	10

[1] Number of pathways in which each gene is involved.

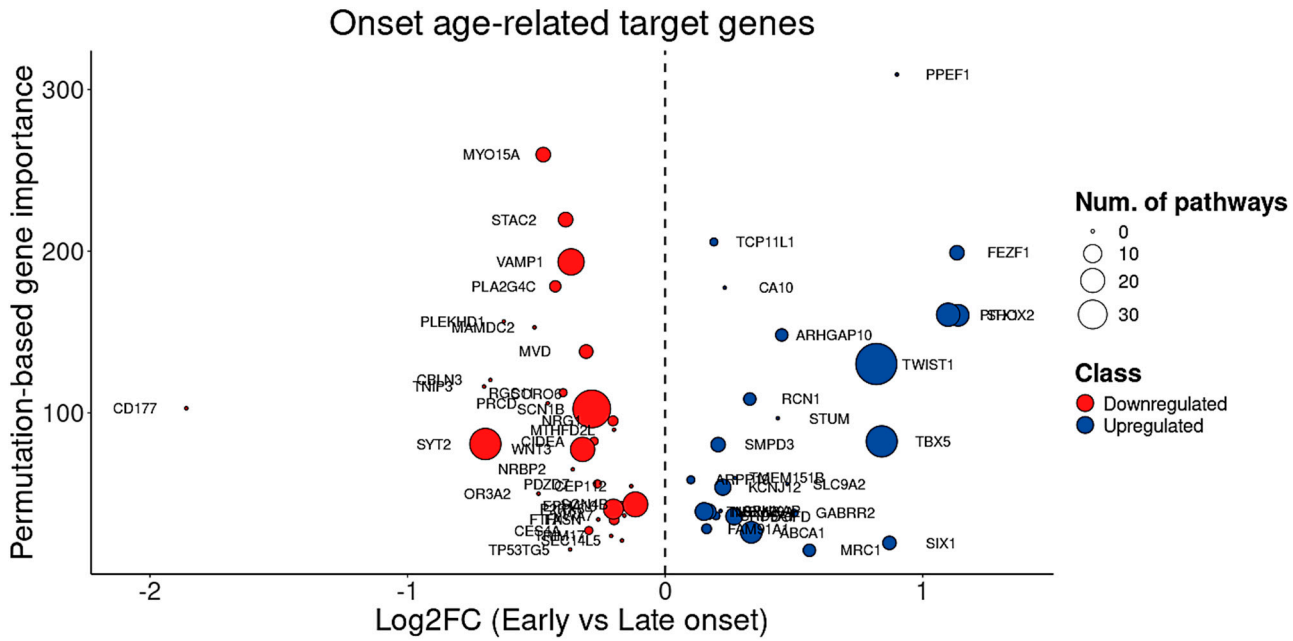

Figure 11. Analysis of the 59 onset age-related target genes showing that, from these genes, 33 are downregulated and 26 are upregulated. Cycle diameter indicates the number of pathways in which each gene is involved. Early onset considered onset age < 35 years whereas late onset considered onset age > 50 years.

Together, these findings underscore the potential of BDASeq® in identifying clinically relevant gene targets that are not only associated with HD pathology but also with key disease-modifying factors such as CAG repeat length and age of symptom onset.

3.8. BDASeq® Identified Target Genes Associated with Brain Degeneration

Analysis of the Vonsattel grade data (available on the metadata of the analyzed BioSamples), revealed that earlier onset age (Figure 12A) and earlier age at death were associated with more severe brain degeneration (Figure 12B). Additionally, increased brain degeneration was correlated with longer CAG repeat (Figure 12C). reinforcing the strong relationship between CAG repeat length and neurodegenerative progression in HD.

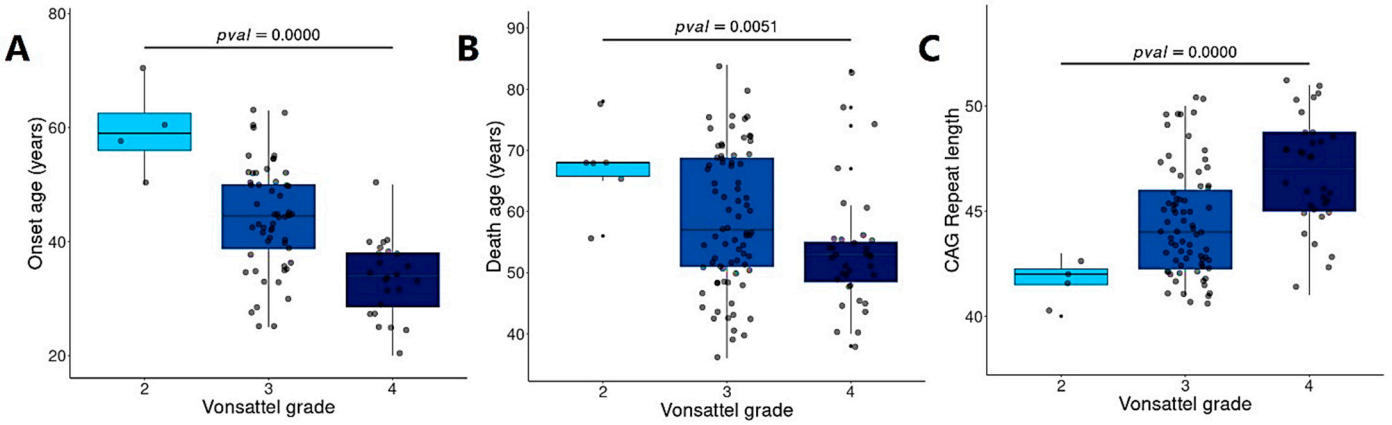

Figure 12. Analysis of brain degeneration based on the Vonsattel grade. Results show that the higher the Vonsattel grade and, therefore, the brain degeneration, the shorter the onset (**A**) and death age (**B**), but the higher the CAG repeat length (**C**). Results were obtained using BDASeq®. Statistical analysis was performed using ANOVA, with a significant level of 5%.

Although BDASeq® identified 12 genes associated with CAG repeat length (Table 5, Figure 13) that could potentially serve as biomarkers, their therapeutic value may be limited. This limitation arises because, despite pharmacological modulation, the persistent expression of *mHTT* may continue to dysregulate these targets, reducing the efficacy of potential therapies due to competitive interference. To address this challenge, the BDASeq® AI algorithm also prioritized gene targets based on their association with Vonsattel grade—a direct indicator of neurodegeneration and indirectly linked to CAG repeat length (Figure 12C). This approach led to the novel identification of 84 brain degeneration-related genes, comprising 47 DRGs and 37 URGs, which may serve as viable therapeutic targets to counter HD-related neurodegeneration (Table 5, Figure 13).

Table 5. Genes identified by the BDASeq® AI algorithm as brain degeneration-related targets.

Gene	Classification	*p*-Value	Log2FC	FDR	Pathways [1]
NUDT18	DRG	0.0060	−0.7345	0.0000	0
CLEC2L	DRG	0.0008	−0.7127	0.0000	0
TIMM23B	DRG	0.0067	−0.4999	0.0013	2
IQANK1	DRG	0.0406	−0.7817	0.0000	0
SMIM10L2B	DRG	0.0309	−0.6233	0.0000	0
KAZN	DRG	0.0084	−0.4590	0.0000	1
PDZD7	DRG	0.0141	−0.5045	0.0000	1
AHNAK2	DRG	0.0372	−0.6515	0.0000	0
NRBP2	DRG	0.0256	−0.4667	0.0000	0
EPHA10	DRG	0.0093	−0.6829	0.0000	2
NXPH4	DRG	0.0339	−1.0172	0.0000	1

Table 5. *Cont.*

Gene	Classification	*p*-Value	Log2FC	FDR	Pathways [1]
SCN4B	DRG	0.0339	−0.5889	0.0000	22
CIDEA	DRG	0.0042	−0.6417	0.0004	1
PLEKHD1	DRG	0.0083	−0.7914	0.0001	0
PHOSPHO1	DRG	0.0406	−0.5368	0.0008	2
CES4A	DRG	0.0444	−0.6246	0.0000	1
LDLRAD4	DRG	0.0075	−0.4421	0.0000	0
HR	DRG	0.0030	−0.7181	0.0000	0
CORO6	DRG	0.0174	−0.4891	0.0000	0
MVD	DRG	0.0192	−0.5133	0.0004	5
NRG1	DRG	0.0142	−0.6523	0.0000	2
ZSCAN1	DRG	0.0093	−0.7667	0.0000	0
RIT2	DRG	0.0406	−0.7547	0.0000	3
TMEM163	DRG	0.0075	−0.5153	0.0001	6
PLBD2	DRG	0.0157	−0.4840	0.0000	0
PCYOX1L	DRG	0.0079	−0.6316	0.0001	0
SYT2	DRG	0.0309	−1.7452	0.0000	37
STAC2	DRG	0.0014	−0.5169	0.0000	6
VAMP1	DRG	0.0030	−0.6175	0.0000	25
KIF12	DRG	0.0484	−0.8271	0.0000	4
ANGPTL2	DRG	0.0233	−0.8151	0.0004	1
ACP2	DRG	0.0192	−0.5411	0.0000	1
KCNC3	DRG	0.0256	−0.5356	0.0000	30
ARHGEF2	DRG	0.0093	−0.4720	0.0000	8
MECR	DRG	0.0038	−0.4410	0.0000	12
SLC30A3	DRG	0.0484	−0.7125	0.0000	6
VIPR1	DRG	0.0115	−0.4111	0.0001	1
SCN1B	DRG	0.0002	−0.5948	0.0000	56
NAPA	DRG	0.0030	−0.4614	0.0000	11
NEFM	DRG	0.0128	−0.6006	0.0000	2
SEC14L5	DRG	0.0038	−0.5010	0.0000	0
NUP93	DRG	0.0128	−0.4756	0.0000	1
GSTZ1	DRG	0.0406	−0.5657	0.0001	1
P2RX6	DRG	0.0173	−0.5360	0.0000	13
MYO15A	DRG	0.0406	−0.5266	0.0000	6
ADAM11	DRG	0.0354	−0.5504	0.0000	4
F7	DRG	0.0060	−0.8341	0.0000	1
SLC5A3	URG	0.0164	0.8459	0.0000	4
HMGN5	URG	0.0256	0.5588	0.0002	2
TOPORS	URG	0.0067	0.4285	0.0001	13
PTAR1	URG	0.0211	0.6316	0.0000	0
PLEKHF2	URG	0.0115	0.6301	0.0000	0
GPR171	URG	0.0067	1.8061	0.0000	2
SLFN11	URG	0.0406	1.0408	0.0000	7
BCL2	URG	0.0060	0.5718	0.0000	95
ARHGAP42	URG	0.0142	0.7404	0.0000	7

Table 5. *Cont.*

Gene	Classification	*p*-Value	Log2FC	FDR	Pathways [1]
STOX1	URG	0.0211	0.5138	0.0000	14
RHOBTB3	URG	0.0192	0.7695	0.0000	2
RANBP3L	URG	0.0157	1.2461	0.0000	5
PPP4R2	URG	0.0309	0.4286	0.0000	4
GRAMD2B	URG	0.0060	0.8249	0.0000	0
GABPA	URG	0.0060	0.4045	0.0002	7
BCL2L11	URG	0.0339	0.5653	0.0002	35
GXYLT1	URG	0.0053	0.4231	0.0002	1
PARD3	URG	0.0339	0.9958	0.0000	8
SLC39A12	URG	0.0233	1.1799	0.0000	5
G3BP1	URG	0.0034	0.4533	0.0000	8
USP53	URG	0.0406	0.8390	0.0000	2
YAP1	URG	0.0115	1.1163	0.0000	57
SLC38A2	URG	0.0173	0.8775	0.0000	8
MAP7D3	URG	0.0030	0.5214	0.0019	0
FEZF1	URG	0.0309	1.6361	0.0000	6
GNA13	URG	0.0104	0.7054	0.0000	15
UPK1B	URG	0.0173	2.6019	0.0000	1
GMNN	URG	0.0339	0.7335	0.0001	9
GABRR2	URG	0.0174	1.3858	0.0000	1
DSE	URG	0.0084	0.9154	0.0000	14
ITGB8	URG	0.0021	0.6760	0.0000	20
ATP11C	URG	0.0371	0.6688	0.0000	1
EZR	URG	0.0406	0.7495	0.0000	20
TGFBR3	URG	0.0211	1.1844	0.0000	34
LAPTM4A	URG	0.0443	0.5393	0.0000	0
IL17RB	URG	0.0173	1.1067	0.0000	5
RCN1	URG	0.0142	0.6193	0.0000	4

[1] Number of pathways in which each gene is involved.

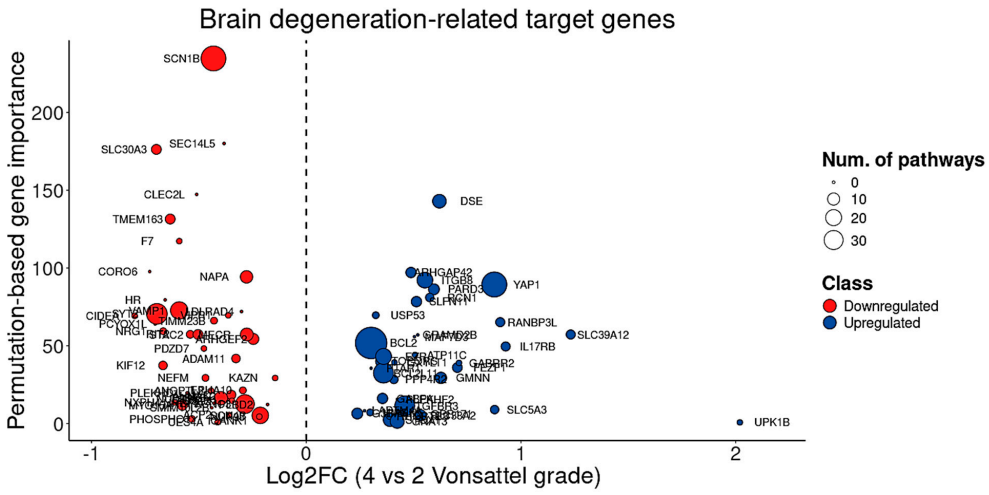

Figure 13. Analysis of the 84 brain degeneration-related target genes showing that, from these genes, 47 are downregulated and 37 are upregulated. Circle diameter indicates the number of pathways in which each gene is involved. In this comparison we used both lower level of degeneration vs. higher level of degeneration (Vonsattel scale 4 vs. 2).

Furthermore, recognizing that both brain degeneration and CAG repeat length correlate with age of death (Figure 12B), this study calculated life expectancy in HD gene-positive individuals as the difference between age of death and age of symptom onset. Using this metric, BDASeq® identified 16 genes—including 13 DRGs and 3 URGs—whose expression is strongly associated with patient lifespan (Table 6, Figure 14). These genes represent promising targets for therapeutic strategies aimed at altering the disease course and extending life expectancy in HD.

Table 6. Genes identified by the BDASeq AI algorithm as lifespan-related targets.

Gene	Classification	*p*-Value	Log2FC	FDR	Pathways [1]
MRC1	DRG	0.0412	1.8902	0.0000	4
STUM	DRG	0.0090	−0.8045	0.0000	0
GAS1	DRG	0.0152	1.0313	0.0001	11
NPAS4	DRG	0.0075	−2.8925	0.0049	0
SPTLC3	DRG	0.0075	1.9498	0.0001	0
S100P	DRG	0.0427	2.4416	0.0000	5
SLC16A12	DRG	0.0112	3.0162	0.0000	2
OSR1	DRG	0.0028	1.3507	0.0036	8
STRA6	DRG	0.0026	1.3572	0.0138	2
CEMIP	DRG	0.0152	0.7861	0.0000	2
FCGR2B	DRG	0.0023	2.3809	0.0000	53
PKP2	DRG	0.0230	1.0042	0.0001	9
MARCO	DRG	0.0128	2.1951	0.0000	3
TMEM163	URG	0.0341	−0.5153	0.0001	6
ANGPT2	URG	0.0165	1.4528	0.0000	17
RIPOR3	URG	0.0427	1.2127	0.0000	0

[1] Number of pathways in which each gene is involved.

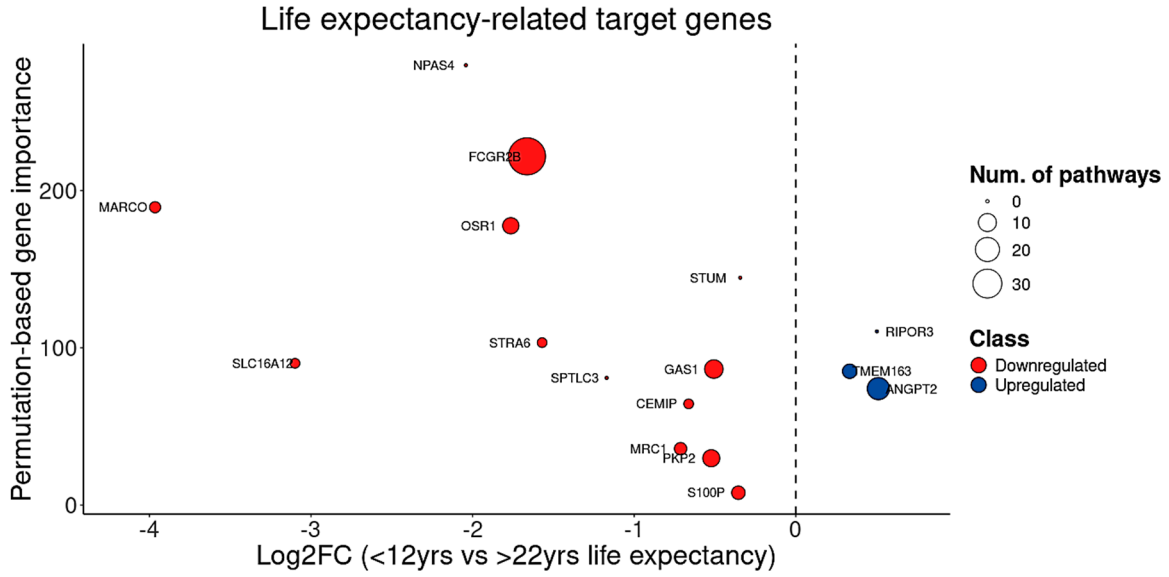

Figure 14. Analysis of the 16 life expectancy-related target genes showing that, from these genes, 13 are downregulated and 3 are upregulated. Circle diameter indicates the number of pathways in which each gene is involved.

3.9. BDASeq® Identified for First-Time Blood Biomarkers for HD, Including FTH1

In the analysis of three additional BioProjects, PRJNA225101 (*n* = 124 BioSamples), PRJNA559372 (*n* = 93 BioSamples), and PRJNA261011 (*n* = 16 BioSamples)—which in-

cluded blood RNA-Seq datasets from HD gene-positive individuals and controls–BDASeq® identified only 20 DEGs in the blood of HD patients (Table 7). However, two of these DEGs are non-coding genes (ENSG00000250568 and ENSG00000260035, Table 7), reducing the number of relevant DEGs to 18 genes. These genes were removed from downstream analysis, once for drug design or diagnosis, protein-coding genes are the primary targets of many drugs and antibodies.

Table 7. Genes identified as DEGs in the blood of HD gene-positive individuals.

Gene ID	Gene	Log2FC	FDR	Classification
ENSG00000250568 [1]	*PABPC1*	1.2687	0.0267	URG
ENSG00000260035	*Lnc-DUOXA1-2*	2.3900	0.0003	URG
ENSG00000149925	*ALDOA*	0.8515	0.0014	URG
ENSG00000141480	*ARRB2*	0.4655	0.0009	URG
ENSG00000135636	*DYSF*	0.6159	0.0109	URG
ENSG00000132589	*FLOT2*	0.4394	0.0369	URG
ENSG00000167996	*FTH1*	1.1435	0.0024	URG
ENSG00000174021	*GNG5*	0.4621	0.0295	URG
ENSG00000170837	*GPR27*	0.6579	0.0127	URG
ENSG00000030582	*GRN*	0.5643	0.0495	URG
ENSG00000248099	*INSL3*	1.4028	0.0014	URG
ENSG00000251230	*MIR3945HG*	0.8796	0.0493	URG
ENSG00000170909	*OSCAR*	0.5463	0.0403	URG
ENSG00000170525	*PFKFB3*	0.8153	0.0006	URG
ENSG00000105287	*PRKD2*	0.4599	0.0077	URG
ENSG00000112053	*SLC26A8*	0.9719	0.0495	URG
ENSG00000266402	*SNHG25*	1.6604	0.0156	URG
ENSG00000184292	*TACSTD2*	3.8049	0.0000	URG
ENSG00000156414	*TDRD9*	1.1963	0.0403	URG
ENSG00000170873	*MTSS1*	−0.6198	0.0011	DRG

[1] Pseudogene.

Among these 18 DEGs, only one gene, *FTH1*, was also identified in the prefrontal and motor cortex of HD in gene-positive individuals (Figure 15A). Interestingly, *FTH1* was found downregulated in a CAG repeat length-dependent manner (Figure 15B) and upregulated in the peripheral blood of HD gene-positive individuals (Figure 15C). As the major subunit of ferritin, FTH1 is responsible for intracellular iron storage and protection against iron-induced oxidative stress. This finding positions FTH1 as a promising candidate for biomarker for HD.

Furthermore, ARRB2 and PFKFB3 are promising biomarker candidates for Huntington's disease (HD) due to their involvement in key pathological processes—*ARRB2* in neuronal signaling and cell death, and *PFKFB3* in glycolytic metabolism and energy stress. Both genes are expressed in the brain, including the prefrontal cortex, and in peripheral blood, which supports their potential for minimally invasive monitoring. Although CAG repeat expansion does not directly regulate *ARRB2* or *PFKFB3*, it induces cellular conditions such as stress, metabolic shifts, and synaptic dysfunction, which in turn affect these genes. Consequently, their altered expression and functional activity may serve as indirect indicators of CAG-induced pathology, reinforcing their potential as biomarkers for HD. Changes in their expression could reflect disease progression and therapeutic response. However, further validation is needed to confirm their specificity and sensitivity within the context of HD.

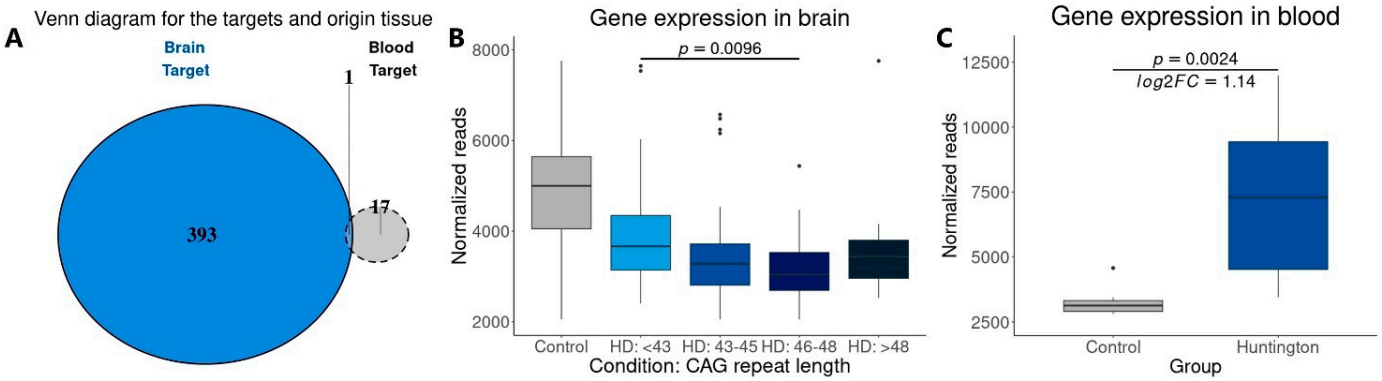

Figure 15. Venn diagram showing that, from the 394 HD targets identified in the prefrontal and motor cortex of HD gene-positive individuals (**A**), only FTH1 was found downregulated (in a CAG-dependent manner) (**B**) in the brain and upregulated in the blood (**C**).

4. Discussion

HD was first reported over 150 years ago, yet it remains without drugs capable of altering its natural history. Current approved treatments, such as tetrabenazine, deutetrabenazine, and valbenazina, provide limited therapeutic benefits, mainly addressing chorea in the early stages of the disease. However, these treatments are associated with multiple adverse effects, including depression, which increases the risk of suicide. The absence of disease-modifying drugs that provide wider therapeutic benefits or postpone neurodegeneration is largely due to the complexity of the disease, the lack of suitable animal models, and the limited number of druggable genes that can be explored through computer-aided drug design (CADD) [16,17]. In this context, RNA-Seq analysis combined with different analytical approaches are a promising tool for identifying potential druggable genes.

To uncover such genes, at least six independent studies have comparatively analyzed the transcriptomes of prefrontal cortex postmortem samples from symptomatic individuals carrying the *mHTT* gene (cases) and neurologically normal controls [75,76,79,80]. These studies focused on prefrontal cortex and caudate nucleus, since about 90% of striatal neurons, primarily affected by the disease, are lost in late-stage HD, making it difficult to study striatal postmortem samples from individuals with HD due to the scarcity of neurons in highly degenerated tissue, as previously discussed by us [18]. However, studies based on structural magnetic resonance imaging (MRI) evidenced that, in late-stage HD, BA9 exhibits loss of projection neurons in layers III, V, and VI and glial density increases in deeper layer (VI) consistent with cortical degeneration [81,82]. These results make BA9 an important brain area to be explored to identify possible pharmacological/prognostic targets for HD [18].

Despite these substantial efforts, the DEGs identified by these studies have not led to the discovery of useful druggable genes or blood biomarkers for HD [75,76,79,80,83,84]. A common theme across these studies is the identification of genes belonging to the heat shock family or genes involved in inflammatory processes as potential therapeutic targets and/or biomarkers [75,76,79,80,83,84].

Reanalyzing the transcriptomic dataset of one of these studies [75], we demonstrated that failure to match cases and controls by age negatively affects DEG identification, leading to an increase in both false positive and false negative errors [18]. Using a PSM algorithm to create an age-matched control group, we were able to identify multiple putative druggable genes involved in HD pathophysiology that do not belong to the heat shock family [18]. Further examination of previously published transcriptomic studies on HD [75,76,79,80,83,84] revealed that differences in bioinformatic pipelines, including various differential expression analysis (DEA) methods, different normalization approaches,

and the small sample sizes, might contribute to the lack of consensus regarding DEGs. To address this limitation, we aggregated RNA-Seq data from multiple studies available in the SRA database, which significantly increased the sample size. This strategy was crucial for DEG identification, given that HD is a heterogeneous disease. Through this approach, we identified 353 pre-eligible BioSamples. Using the PSM function in BDASeq®, we obtained 292 eligible BioSamples (146 age-matched controls, and 146 cases) for further analysis, making this the largest transcriptomic study on HD compiled into data, as recognized by the International Huntington Association (IHA), Brazil Huntington Association (ABH), and *Fundação de Amparo à Pesquisa do Estado de São Paulo* (FAPESP, available on https://agencia.fapesp.br/a-startup-supported-by-fapesp-is-conducting-one-of-the-largest-studies-on-huntingtons-disease/51647, accessed on 23 June 2025).

Applying the RMC algorithm, BDASeq® identified 5834 DEGs, including 394 putative druggable genes in the prefrontal and motor cortex of HD-positive individuals. Comparative analysis of the expression levels (read counts) of these 394 genes confirmed their differential expression in the prefrontal cortex of HD patients. Functional enrichment analysis revealed that these 394 putative therapeutic targets are involved in key HD-related pathophysiological processes, including metal ion dysregulation, cholesterol metabolism disruption, neuroinflammation, impaired blood–brain barrier transport, neurotransmission dysfunction, and axon guidance disturbances. These results suggest that BDASeq® effectively identified candidate genes for therapeutic targeting in HD.

In addition, BDASeq® also highlighted potential therapeutic target genes whose expression levels are associated with CAG repeat length, onset age, Vonsattel grade (or brain degeneration), and lifespan. Although further validation is required to confirm their role in these processes, these genes hold promise for drug design or repositioning to provide broader therapeutic benefits than those offered by current drugs like tetrabenazine, deutetrabenazine, or valbenazine, as well as investigational compounds like pridopidine, which are focused solely on chorea.

In the context of drug development, a significant challenge, particularly in clinical trials, is demonstrating the efficacy of investigational products. This challenge is compounded by the lack of reliable biomarkers, which restrict efficacy assessments to subjective measures like the Unified Huntington's Disease Rating Scale (UHDRS). While the UHDRS' Total Motor Score (TMS) and Total Functional Capacity (TFC) assessments are widely used and have acceptable interrater reliability, they ultimately depend on the clinical experience of the rater and lack precision in certain contexts. Therefore, the discovery of HD biomarkers is crucial for improving clinical trial outcomes.

Ideally, a biomarker should be a biomolecule whose expression is differentially regulated under pathological conditions and can be easily monitored in accessible tissues, preferably peripheral blood [85].

Several studies have aimed to identify HD biomarkers in the peripheral blood of HD gene-positive individuals [83,84,86]. However, these studies have not yielded useful biomarkers, as pointed out by Mitchell et al. [85] in the TRACK-HD study. This failure can be attributed to a lack of advanced analytical technologies that combine AI and bioinformatics to integrate transcriptomic data with clinical–pathological features. In our study, we also analyzed three additional BioProjects containing transcriptomic data from the blood of HD gene-positive individuals. BDASeq® identified 18 potential blood biomarkers. Interestingly, only one of these biomarkers (*FTH1*) was found among the 394 potential therapeutic targets differentially expressed in the prefrontal cortex of HD individuals.

Recent studies highlight *PFKFB3* and *ARRB2* as potential biomarkers and therapeutic targets in HD. *PFKFB3*, a regulator of glycolytic metabolism, is implicated in neurodegenerative diseases like Alzheimer's, where it affects amyloid-beta accumulation and neuronal

dysfunction [87]. In HD, its expression may reflect metabolic shifts and neuronal stress. Similarly, *ARRB2* (Beta-Arrestin 2) is involved in neurodegeneration by interacting with pathways linked to protein accumulation, such as amyloid-beta in Alzheimer's and tau in frontotemporal dementia. *ARRB2* also influences neuroinflammation, synaptic dysfunction, and may regulate alpha-synuclein in Parkinson's disease, suggesting a similar role in HD [88]. Additionally, *ARRB2* mediates dopaminergic signaling in the hippocampus, which is relevant to HD pathology [89]. Together, these genes contribute to key mechanisms in HD, including cellular stress, metabolic dysfunction, and protein aggregation, supporting their potential as biomarkers and therapeutic targets. However, further research is needed to validate their role in HD.

Given that an ideal biomarker should be differentially expressed in both the primary tissue affected by the disease but also be differentially expressed in peripheral blood, with its expression linked to disease phenotype or pathophysiological processes [85], FTH1 emerges as a promising biomarker for HD. The FTH1 gene was found in the prefrontal cortex in a CAG repeat length-dependent manner but upregulated in the peripheral blood of HD gene-positive individuals.

The *FTH1* gene encodes the ferritin have chain 1 (FTH1), a critical protein involved in iron homeostasis [90]. FTH1 acts as the primary cytosolic iron storage protein, buffering against oxidative stress [91]. Elevated levels of FTH1 helps maintain iron balance and mitochondrial homeostasis, protecting cells, including neurons, from oxidative stress [91]. FTH1 is also involved in innate immune system pathways by regulating iron levels and influencing inflammation [91]. In addition, FTH1 is involved in vesicle transport in neurons, particularly in iron storage and neuron survival [92].

Exosomes secreted by oligodendrocytes, which carry FTH1, provide antioxidant protection to neurons against iron-induced cytotoxicity [92]. Interestingly, recent studies have shown that exosomes play a role in iron transport across the blood–brain barrier [93], which may explain the compensatory upregulation of FTH1 observed in the blood of HD-positive individuals.

In HD, FTH1 is associated with ferroptosis, a form of iron-dependent cell death driven by lipid peroxidation, as revised by Jamal et al. [94]. Interesting, downregulation of FTH1 has also been reported as a key mediator of ferroptosis and oxidative stress in other neurodegenerative diseases, such as Parkinson's (PD) and Alzheimer's disease (AD) [94–97]. Consistent with these findings, Li et al. [98] showed that miR-335 promotes ferroptosis in vitro and in vivo models for PD by targeting *FTH1*.

Although serum ferritin levels have been investigated in HD for over three decades [99,100], these studies typically measure total ferritin protein, which may explain the discrepancies observed, with some studies reporting decreased ferritin levels [99,100], while our study shows *FTH1* upregulation in peripheral blood. This highlights the potential of FTH1 as a novel biomarker for HD. However, further studies using qRT-PCR to assess *FTH1* expression and immunoassays to measure FTH1 levels are needed to validate its utility as a biomarker for HD.

5. Conclusions

In conclusion, this study demonstrates the effectiveness of different analytical strategies and methods, consisting of the BDASeq®, in identifying potential therapeutic targets and biomarkers for HD through a comprehensive transcriptomic analysis. The application of PSM and aggregation of RNA-Seq data from multiple studies allowed for a robust identification of 394 druggable genes, which are implicated in key HD-related processes such as neuroinflammation, metal ion dysregulation, and impaired blood–brain barrier transport. Among these, FTH1 stands out as a promising biomarker due to its differential expression

in both the prefrontal cortex and peripheral blood of HD gene-positive individuals. The upregulation of FTH1 in peripheral blood, combined with its role in iron homeostasis and neuroprotection, underscores its potential as a novel biomarker for HD. This finding is further supported by its involvement in ferroptosis, a form of cell death linked to oxidative stress in neurodegenerative diseases. Despite these promising results, further validation using techniques like qRT-PCR and immunoassays is needed to establish FTH1's clinical utility as a biomarker for HD. Ultimately, the identification of these genes offers valuable insights into the development of disease-modifying treatments and biomarkers that could enhance clinical trial outcomes and improve patient care in HD.

6. Patents

BDASeq® is a computer program developed by BioDecision Analytics™. (João Rafael Dias Pinto, Rodrigo Pinheiro Araldi, and Benedito Faustinoni Neto) and registered in the Brazilian National Institute of Industrial Property (INPI, BR512025001097-4).

Supplementary Materials: The following supporting information can be downloaded at: https://www.mdpi.com/article/10.3390/cells14130976/s1, File S1—BioSample metadata. File S2—List of differentially expressed genes (DEGs) identified using BDASeq®. File S3—List of target genes identified using AI. File S4—Functional enrichment analysis of target genes.

Author Contributions: Conceptualization, J.R.D.P., B.F.N., and R.P.A.; methodology, J.R.D.P., B.F.N., and R.P.A.; software, J.R.D.P., B.F.N., and R.P.A., validation, J.R.D.P., B.F.N., and R.P.A.; formal analysis, J.R.D.P., B.F.N., R.P.A., I.K., and L.M. investigation, J.R.D.P., B.F.N., and R.P.A.; resources, J.R.D.P., B.F.N., and R.P.A.; data curation, J.R.D.P.; writing—original draft preparation, J.R.D.P., B.F.N., R.P.A., I.K., and L.M.; writing—review and editing, J.R.D.P., B.F.N., R.P.A., I.K., and L.M. visualization, J.R.D.P.; supervision, J.R.D.P., R.P.A., and I.K.; project administration, R.P.A. and I.K.; funding acquisition, J.R.D.P. and R.P.A. All authors have read and agreed to the published version of the manuscript.

Funding: This research was funded by Fundação de Amparo à Pesquisa do Estado de São Paulo (FAPESP), grant numbers 2023/06116-2, 2023/10353-0, 2024/07829-5, and 2024/17577-3.

Institutional Review Board Statement: Ethical review and approval were waived for this study since it employs transcriptomic data from a public repository (SRA database). The identity of all subjects is preserved, according to the SRA rules.

Informed Consent Statement: Not applicable.

Data Availability Statement: RNA sequencing files analyzed in this study are available on the SRA database (https://www.ncbi.nlm.nih.gov/sra, accessed on 15 June 2024).

Acknowledgments: The authors thank the support of International Huntington Association (IHA), Brazil Huntington Association (ABH), Brazil Huntington Union House (CBUA), Brazilian Alzheimer's Federation (Febraz), and SINDUSFARMA for this study.

Conflicts of Interest: The authors J.R.D.P., R.P.A., and B.F.N. declare conflicts of interest with BioDecision Analytics™. J.R.D.P., R.P.A., and B.F.N. are inventors of BDASeq®, a computer program developed and registered in Brazil (registration number BR512025001097-4). Supporting funding obtained for this study was obtained for J.R.D.P., R.P.A., and B.F.N. (BioDecision Analytics Ltd.). J.R.D.P., R.P.A. and B.F.N have been involved as consultants in BioDecision Analytics™.

Abbreviations

The following abbreviations are used in this manuscript:

ABH	Brazil Huntington Association
AD	Alzheimer's Disease
BDASeq®	Biomarker Discovery Algorithm

CADD	Computer-aided Drug Design
CAG	Cytosine–Adenine–Guanine
DEA	Differential Expression Analysis
DEG	Differentially Expressed Gene
FTH1	Ferritin Have Chain 1
HD	Huntington's Disease
IHA	International Huntington Association
PD	Parkinson's Disease
PSM	Propensity Score Matching
RMC	Recursive Method Combination
TFC	Total Function Capacity
TMS	Total Motor Score
UHDRS	Unified Huntington's Disease Rate Scale

Appendix A Appendix

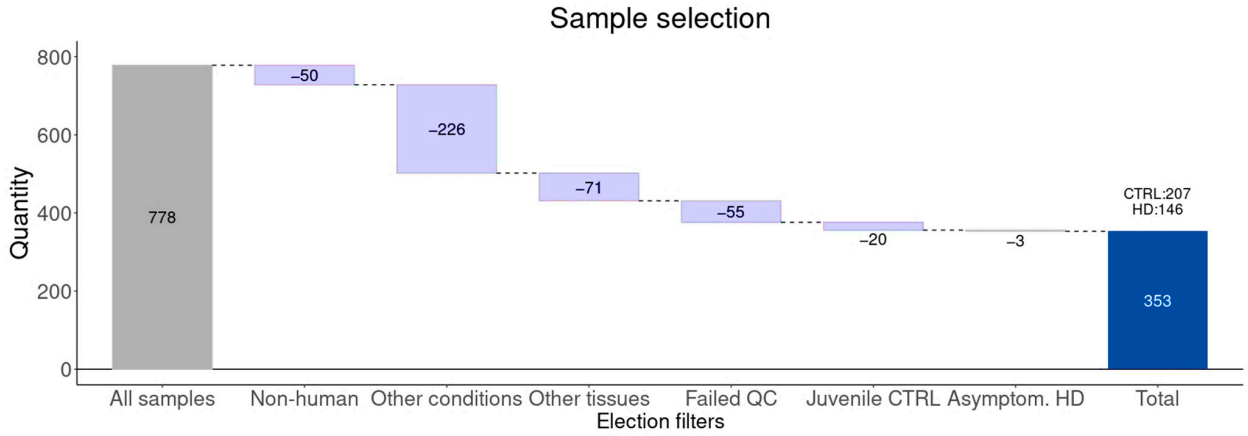

Figure A1. Waterfall plot showing the total number of available brain BioSamples (FASTQ files, n = 778, in grey) included in the 12 BioProjects, as well as the final number of eligible BioSamples (n = 353, in blue) in this study. Note that 425 BioSamples were excluded (jn purple). From the 353 eligible BioSamples, there are 207 BioSamples from neurologically normal individuals (n = 207) and 146 BioSamples from HD-positive symptomatic individuals (n = 146). Doted line describes the reduction in number of samples due to the removal of non-eligible BioSamples.

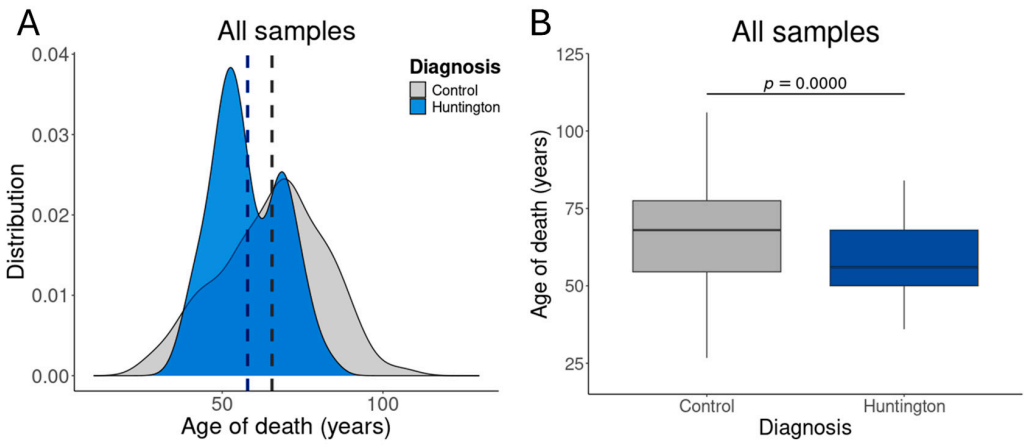

Figure A2. Age distribution between cases (n = 146) and controls (n = 207), (**A**). Results show a statistically significant difference between the age of cases and controls (**B**). Statistical analysis performed using t-Student test, with a significance level of 5%. Doted lines show the mean of each sample distribution.

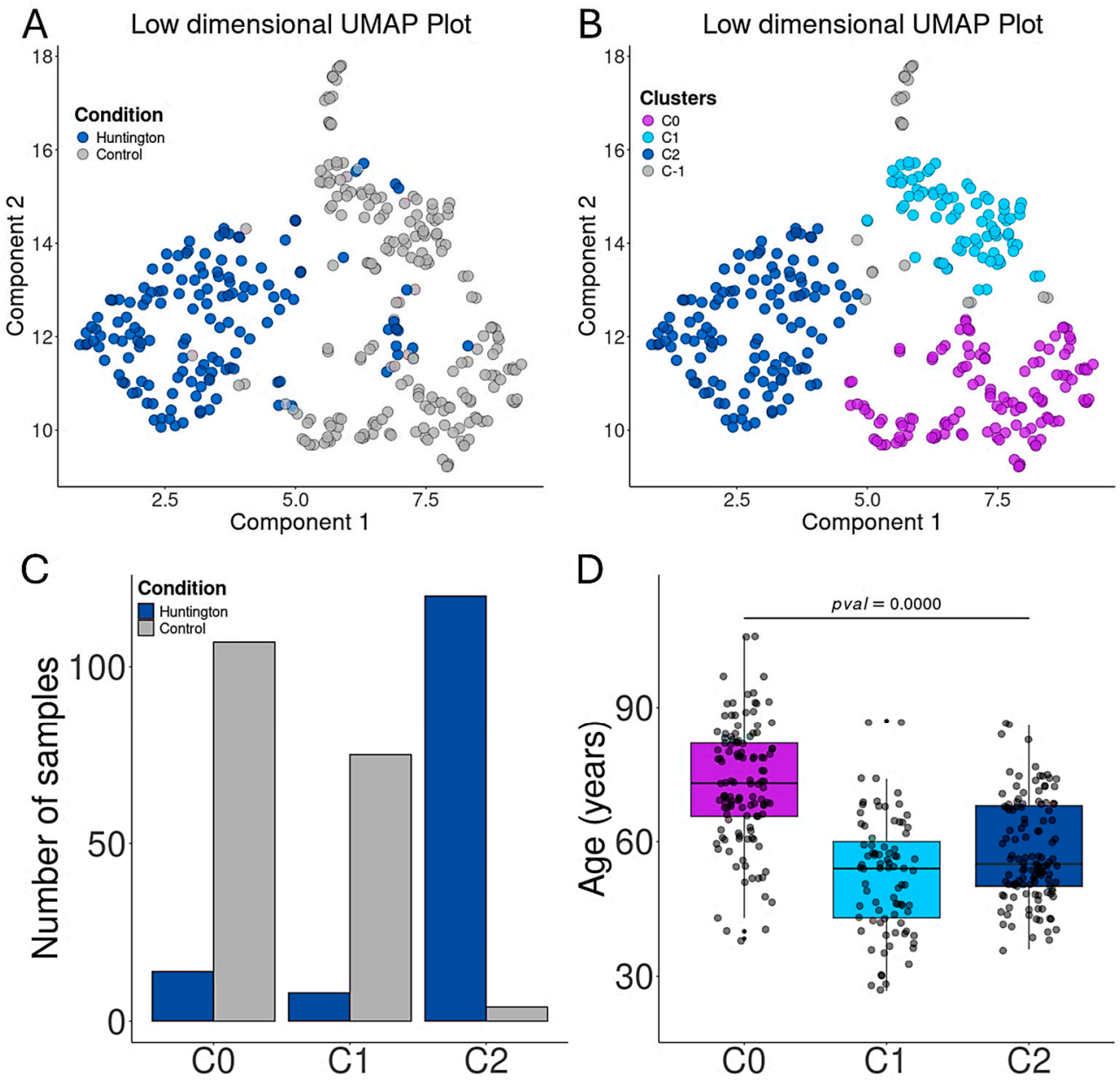

Figure A3. Dimensional reduction analysis through the UMAP technique, showing that transcriptomic profiles from HD-positive individuals (in blue, n = 146) differ from neurologically normal controls (in gray, n = 207), (**A**). Clustering analysis using DBSCAN shows the analyzed transcriptomic profiles grouped into three distinct clusters (**B**). Clustering analysis shows that clusters zero (C0) and one (C1) mostly comprised transcriptomic profiles from neurologically normal controls, whereas cluster two (C2) mostly contains transcriptomic profiles from HD-positive individuals (**C**). Although the sample composition of C0 and C1 are very similar, note that C0 contains older neurologically normal controls than C1, confirming that aging promotes transcriptional changes in the prefrontal cortex (**D**). The C1 group is formed only for samples that cannot be grouped into clusters, which the method identifies as outliers. Statistical analysis was performed using one-way ANOVA followed by Tukey post hoc test, both with significance levels of 5%.

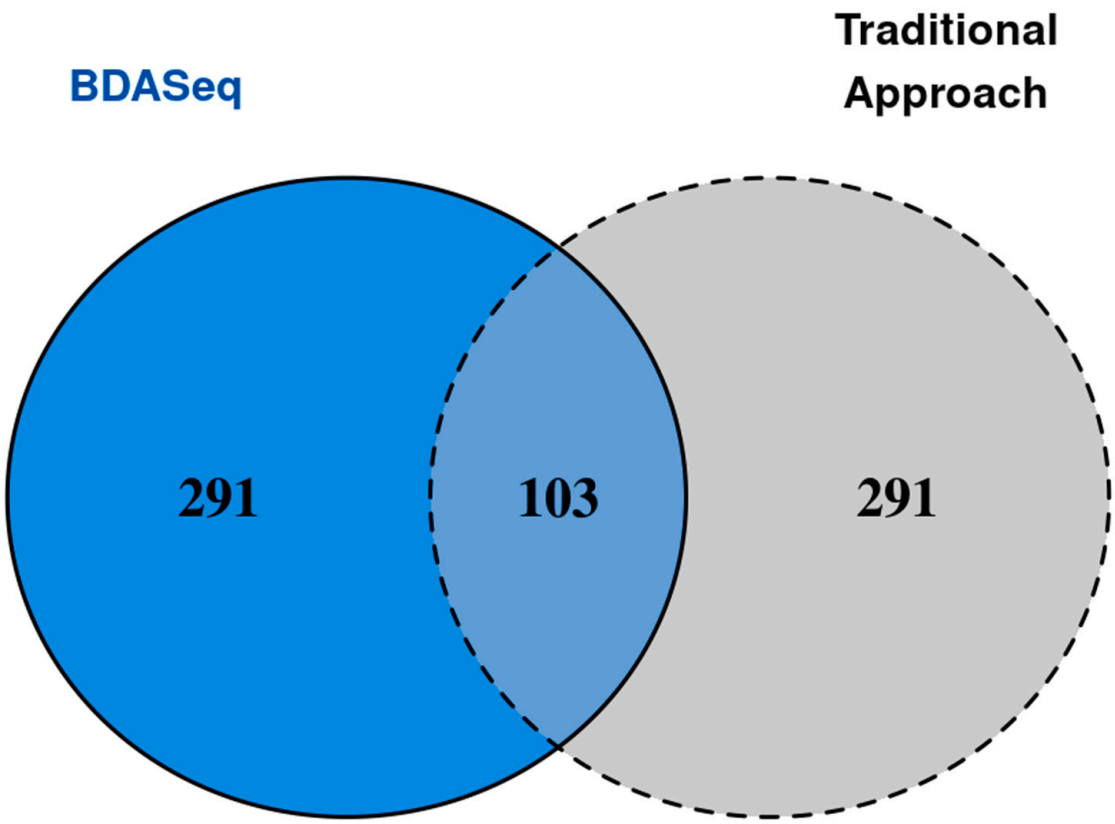

Figure A4. Venn diagram comparing the target genes identified using BDASeq® and traditional pipeline using DESeq2. Note that, from the 394 target genes identified using BDASeq®, only 103 genes could be identified using DESeq2. Results also show that BDASeq® identified 291 novel target genes not identified using traditional approach.

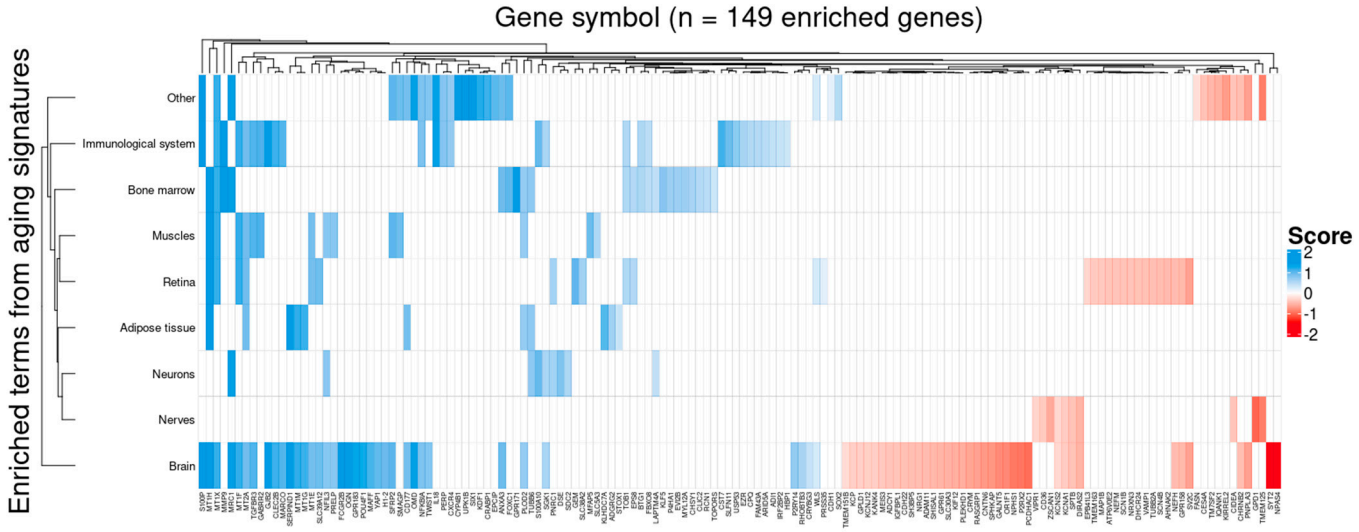

Figure A5. Heatmap showing that 149 of the 394 target genes identified by BDASeq are involved in aging signatures of the brain, muscle, retina, bone marrow, and immunological system, supporting the argument that HD exacerbates aging process. Results obtained using data from the Enrichr web service.

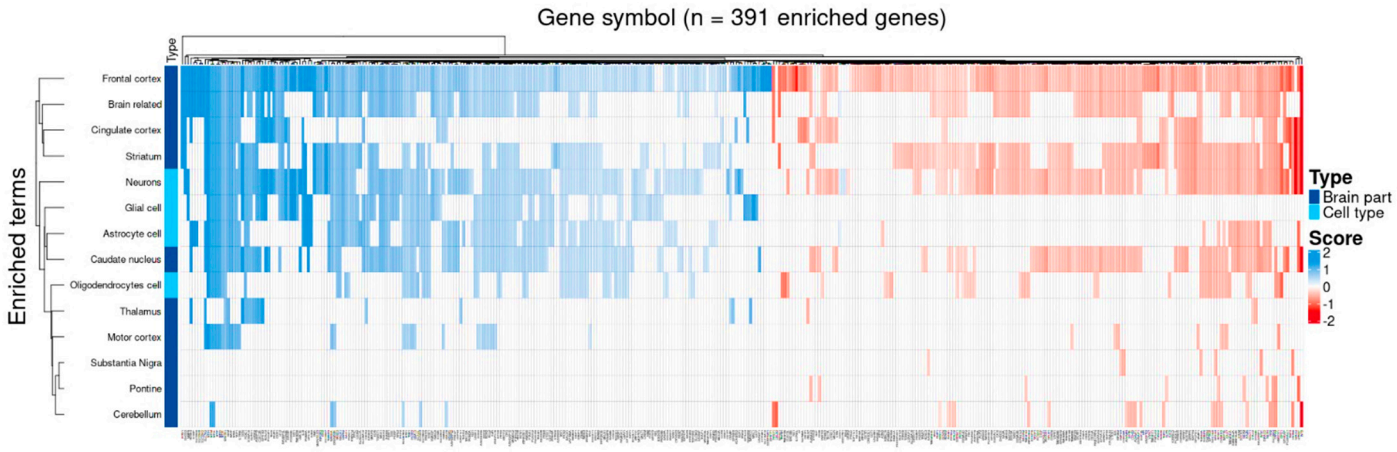

Figure A6. Heatmap showing that 391 of the 394 target genes identified by BDASeq are encoded by different brain areas committed by HD. As expected, most of these genes are encoded in a prefrontal cortex, corresponding to the sequenced area. However, a part of these target genes is deregulated in the striatum (primary committed site by the mHTT-related neurodegeneration), cingulate cortex, and caudate nucleus. Results were obtained using data from the Enrichr web service.

References

1. Medina, A.; Mahjoub, Y.; Shaver, L.; Pringsheim, T. Prevalence and Incidence of Huntington's Disease: An Updated Systematic Review and Meta-Analysis. *Mov. Disord.* **2022**, *37*, 2327–2335. [CrossRef] [PubMed]
2. Jurcau, A.; Jurcau, C. Mitochondria in Huntington's Disease: Implications in Pathogenesis and Mitochondrial-Targeted Therapeutic Strategies. *Neural Regen. Res.* **2023**, *18*, 1472. [CrossRef]
3. Harper, P.S. The Epidemiology of Huntington's Disease. *Hum. Genet.* **1992**, *89*, 365–376. [CrossRef] [PubMed]
4. Bhattacharyya, K. The Story of George Huntington and His Disease. *Ann. Indian Acad. Neurol.* **2016**, *19*, 25. [CrossRef] [PubMed]
5. Macdonald, M. A Novel Gene Containing a Trinucleotide Repeat That Is Expanded and Unstable on Huntington's Disease Chromosomes. *Cell* **1993**, *72*, 971–983. [CrossRef]
6. Claassen, D.O.; Ayyagari, R.; Garcia-Horton, V.; Zhang, S.; Alexander, J.; Leo, S. Real-World Adherence to Tetrabenazine or Deutetrabenazine Among Patients With Huntington's Disease: A Retrospective Database Analysis. *Neurol. Ther.* **2022**, *11*, 435–448. [CrossRef]
7. Furr Stimming, E.; Claassen, D.O.; Kayson, E.; Goldstein, J.; Mehanna, R.; Zhang, H.; Liang, G.S.; Haubenberger, D.; Adams, J.; Beck, C.; et al. Safety and Efficacy of Valbenazine for the Treatment of Chorea Associated with Huntington's Disease (KINECT-HD): A Phase 3, Randomised, Double-Blind, Placebo-Controlled Trial. *Lancet Neurol.* **2023**, *22*, 494–504. [CrossRef]
8. Heim, B.; Seppi, K. Valbenazine as Treatment for Huntington's Disease Chorea. *Lancet Neurol.* **2023**, *22*, 459–460. [CrossRef]
9. Kaur, N.; Kumar, P.; Jamwal, S.; Deshmukh, R.; Gauttam, V. Tetrabenazine: Spotlight on Drug Review. *Ann. Neurosci.* **2016**, *23*, 176–185. [CrossRef]
10. Rodrigues, F.B.; Duarte, G.S.; Costa, J.; Ferreira, J.J.; Wild, E.J. Tetrabenazine Versus Deutetrabenazine for Huntington's Disease: Twins or Distant Cousins? *Mov. Disord. Clin. Pract.* **2017**, *4*, 582–585. [CrossRef]
11. Frank, S.; Testa, C.; Edmondson, M.C.; Goldstein, J.; Kayson, E.; Leavitt, B.R.; Oakes, D.; O'Neill, C.; Vaughan, C.; Whaley, J.; et al. The Safety of Deutetrabenazine for Chorea in Huntington Disease: An Open-Label Extension Study. *CNS Drugs* **2022**, *36*, 1207–1216. [CrossRef] [PubMed]
12. Login, I.S.; Cronin, M.J.; MacLeod, R.M. Tetrabenazine Has Properties of a Dopamine Receptor Antagonist. *Ann. Neurol.* **1982**, *12*, 257–262. [CrossRef]
13. Claassen, D.O.; Carroll, B.; De Boer, L.M.; Wu, E.; Ayyagari, R.; Gandhi, S.; Stamler, D. Indirect Tolerability Comparison of Deutetrabenazine and Tetrabenazine for Huntington Disease. *J. Clin. Mov. Disord.* **2017**, *4*, 3. [CrossRef]
14. Shahani, L. Tetrabenazine and Suicidal Ideation. *J. Neuropsychiatry Clin. Neurosci.* **2013**, *25*, E30. [CrossRef]
15. Dalton, M.P.; Cheng, M.H.; Bahar, I.; Coleman, J. Structural Mechanisms for VMAT2 Inhibition by Tetrabenazine. *Biophys. J.* **2024**, *123*, 116a. [CrossRef]
16. Niazi, S.K.; Mariam, Z. Computer-Aided Drug Design and Drug Discovery: A Prospective Analysis. *Pharmaceuticals* **2023**, *17*, 22. [CrossRef]
17. Faustinoni-Neto, B.; Dias-Pinto, J.R.; Araldi, R.P. Pharma Data Analytics (Pharma Intelligence): Opportunities and Challenges in the Multi-Omics Era of Drug Discovery and Development. *Pharmacologia* **2023**, *14*, 29–39. [CrossRef]

18. Dias-Pinto, J.R.; Faustinoni-Neto, B.; Sanches-Fernandes, J.M.; Kerkis, I.; Araldi, R.P. How Does the Age of Control Individuals Hinder the Identification of Target Genes for Huntington's Disease? *Front. Genet.* **2024**, *15*, 1377237. [CrossRef] [PubMed]
19. Stark, R.; Grzelak, M.; Hadfield, J. RNA Sequencing: The Teenage Years. *Nat. Rev. Genet.* **2019**, *20*, 631–656. [CrossRef]
20. Maza, E. In Papyro Comparison of TMM (EdgeR), RLE (DESeq2), and MRN Normalization Methods for a Simple Two-Conditions-Without-Replicates RNA-Seq Experimental Design. *Front. Genet.* **2016**, *7*, 164. [CrossRef]
21. Zhao, Y.; Li, M.-C.; Konaté, M.M.; Chen, L.; Das, B.; Karlovich, C.; Williams, P.M.; Evrard, Y.A.; Doroshow, J.H.; McShane, L.M. TPM, FPKM, or Normalized Counts? A Comparative Study of Quantification Measures for the Analysis of RNA-Seq Data from the NCI Patient-Derived Models Repository. *J. Transl. Med.* **2021**, *19*, 269. [CrossRef] [PubMed]
22. Love, M.I.; Huber, W.; Anders, S. Moderated Estimation of Fold Change and Dispersion for RNA-Seq Data with DESeq2. *Genome Biol.* **2014**, *15*, 550. [CrossRef]
23. Dias-Pinto, J.R.; Araldi, R.P.; Faustinoni-Neto, B. Biomarker Discovery Algorithm (BDASeq): An Integrative Analytics-Based Tool Designed to Identify Potential Diagnostic and Therapeutic Targets for Diseases. *MENA Congr. Rare Dis.* **2025**, 1.
24. Dias-Pinto, J.R.; Faustinoni-Neto, B.; Araldi, R.P. BDASeq: A Novel and Poweful Tool Able to Accurately Discover Theraeputic Targets for the Treatment of Rare Diseases. In Proceedings of the MENA Rare Disease Congress, Abu Dhabi, United Arab Emirates, 16–19 May 2024; p. 5.
25. Andrews, S. *FastQC: A Quality Control Tool for High Throughput Sequence Data*. 2010. Available online: https://www.bioinformatics.babraham.ac.uk/projects/fastqc/ (accessed on 23 June 2025).
26. Ewels, P.; Magnusson, M.; Lundin, S.; Käller, M. MultiQC: Summarize Analysis Results for Multiple Tools and Samples in a Single Report. *Bioinformatics* **2016**, *32*, 3047–3048. [CrossRef] [PubMed]
27. Dobin, A.; Davis, C.A.; Schlesinger, F.; Drenkow, J.; Zaleski, C.; Jha, S.; Batut, P.; Chaisson, M.; Gingeras, T.R. STAR: Ultrafast Universal RNA-Seq Aligner. *Bioinformatics* **2013**, *29*, 15–21. [CrossRef]
28. Liao, Y.; Smyth, G.K.; Shi, W. FeatureCounts: An Efficient General Purpose Program for Assigning Sequence Reads to Genomic Features. *Bioinformatics* **2014**, *30*, 923–930. [CrossRef] [PubMed]
29. Robinson, M.D.; McCarthy, D.J.; Smyth, G.K. EdgeR: A Bioconductor Package for Differential Expression Analysis of Digital Gene Expression Data. *Bioinformatics* **2010**, *26*, 139–140. [CrossRef]
30. Ritchie, M.E.; Phipson, B.; Wu, D.; Hu, Y.; Law, C.W.; Shi, W.; Smyth, G.K. Limma Powers Differential Expression Analyses for RNA-Sequencing and Microarray Studies. *Nucleic Acids Res.* **2015**, *43*, e47. [CrossRef]
31. Tarazona, S.; García, F.; Ferrer, A.; Dopazo, J.; Conesa, A. NOIseq: A RNA-Seq Differential Expression Method Robust for Sequencing Depth Biases. *EMBnet J.* **2012**, *17*, 18. [CrossRef]
32. Leng, N.; Dawson, J.A.; Thomson, J.A.; Ruotti, V.; Rissman, A.I.; Smits, B.M.G.; Haag, J.D.; Gould, M.N.; Stewart, R.M.; Kendziorski, C. EBSeq: An Empirical Bayes Hierarchical Model for Inference in RNA-Seq Experiments. *Bioinformatics* **2013**, *29*, 1035–1043. [CrossRef]
33. Gauthier, M.; Agniel, D.; Thiébaut, R.; Hejblum, B.P. Dearseq: A Variance Component Score Test for RNA-Seq Differential Analysis That Effectively Controls the False Discovery Rate. *NAR Genom. Bioinform.* **2020**, *2*, lqaa093. [CrossRef] [PubMed]
34. Wilcoxon, F. Individual Comparisons by Ranking Methods. *Biom. Bull.* **1945**, *1*, 80. [CrossRef]
35. Firth, D. Bias Reduction of Maximum Likelihood Estimates. *Biometrika* **1993**, *80*, 27–38. [CrossRef]
36. Rosenbaum, P.R.; Rubin, D.B. The Central Role of the Propensity Score in Observational Studies for Causal Effects. *Biometrika* **1983**, *70*, 41–55. [CrossRef]
37. Walsh, M.C.; Trentham-Dietz, A.; Newcomb, P.A.; Gangnon, R.; Palta, M. Using Propensity Scores to Reduce Case-Control Selection Bias. *Epidemiology* **2012**, *23*, 772–773. [CrossRef]
38. Araldi, R.P.; Faustinoni-Neto, B.; Dias-Pinto, J.R. Novel Pharmaceutical Tragets and Prognostic Biomarkers for Huntington's Disease: New Perspectives for the Drug Development. In Proceedings of the MENA Rare Disease Congress, Abu Dhabi, United Arab Emirates, 16–19 May 2024; p. 4.
39. Ho, D.E.; Imai, K.; King, G.; Stuart, E.A. Matching as Nonparametric Preprocessing for Reducing Model Dependence in Parametric Causal Inference. *Political Anal.* **2007**, *15*, 199–236. [CrossRef]
40. Conesa, A.; Madrigal, P.; Tarazona, S.; Gomez-Cabrero, D.; Cervera, A.; McPherson, A.; Szcześniak, M.W.; Gaffney, D.J.; Elo, L.L.; Zhang, X.; et al. A Survey of Best Practices for RNA-Seq Data Analysis. *Genome Biol.* **2016**, *17*, 13. [CrossRef]
41. Zhang, Y.; Parmigiani, G.; Johnson, W.E. ComBat-Seq: Batch Effect Adjustment for RNA-Seq Count Data. *NAR Genom. Bioinform.* **2020**, *2*, lqaa078. [CrossRef]
42. Akond, Z.; Alam, M.; Mollah, M.N.H. Biomarker Identification from RNA-Seq Data Using a Robust Statistical Approach. *Bioinformation* **2018**, *14*, 153–163. [CrossRef]
43. Amaratunga, D.; Göhlmann, H.; Peeters, P.J. Microarrays. In *Comprehensive Medicinal Chemistry II*; Elsevier: Amsterdam, The Netherlands, 2007; pp. 87–106.
44. Pfalzer, A.C.; Yan, Y.; Kang, H.; Totten, M.; Silverman, J.; Bowman, A.B.; Erikson, K.; Claassen, D.O. Alterations in Metal Homeostasis Occur Prior to Canonical Markers in Huntington Disease. *Sci. Rep.* **2022**, *12*, 10373. [CrossRef]

45. Fox, J.H.; Kama, J.A.; Lieberman, G.; Chopra, R.; Dorsey, K.; Chopra, V.; Volitakis, I.; Cherny, R.A.; Bush, A.I.; Hersch, S. Mechanisms of Copper Ion Mediated Huntington's Disease Progression. *PLoS ONE* **2007**, *2*, e334. [CrossRef]
46. Rosas, H.D.; Chen, Y.I.; Doros, G.; Salat, D.H.; Chen, N.; Kwong, K.K.; Bush, A.; Fox, J.; Hersch, S.M. Alterations in Brain Transition Metals in Huntington Disease. *Arch. Neurol.* **2012**, *69*, 887–893. [CrossRef]
47. Cordeiro, L.M.; Soares, M.V.; da Silva, A.F.; dos Santos, L.V.; de Souza, L.I.; da Silveira, T.L.; Baptista, F.B.O.; de Oliveira, G.V.; Pappis, C.; Dressler, V.L.; et al. Toxicity of Copper and Zinc Alone and in Combination in Caenorhabditis Elegans Model of Huntington's Disease and Protective Effects of Rutin. *Neurotoxicology* **2023**, *97*, 120–132. [CrossRef]
48. Kacher, R.; Mounier, C.; Caboche, J.; Betuing, S. Altered Cholesterol Homeostasis in Huntington's Disease. *Front. Aging Neurosci.* **2022**, *14*, 797220. [CrossRef]
49. Leoni, V.; Caccia, C. The Impairment of Cholesterol Metabolism in Huntington Disease. *Biochim. Biophys. Acta (BBA)-Mol. Cell Biol. Lipids* **2015**, *1851*, 1095–1105. [CrossRef] [PubMed]
50. Karasinska, J.M.; Hayden, M.R. Cholesterol Metabolism in Huntington Disease. *Nat. Rev. Neurol.* **2011**, *7*, 561–572. [CrossRef]
51. Jia, Q.; Li, S.; Li, X.-J.; Yin, P. Neuroinflammation in Huntington's Disease: From Animal Models to Clinical Therapeutics. *Front. Immunol.* **2022**, *13*, 1088124. [CrossRef] [PubMed]
52. Björkqvist, M.; Wild, E.J.; Thiele, J.; Silvestroni, A.; Andre, R.; Lahiri, N.; Raibon, E.; Lee, R.V.; Benn, C.L.; Soulet, D.; et al. A Novel Pathogenic Pathway of Immune Activation Detectable before Clinical Onset in Huntington's Disease. *J. Exp. Med.* **2008**, *205*, 1869–1877. [CrossRef] [PubMed]
53. Silvestroni, A.; Faull, R.L.M.; Strand, A.D.; Möller, T. Distinct Neuroinflammatory Profile in Post-Mortem Human Huntington's Disease. *Neuroreport* **2009**, *20*, 1098–1103. [CrossRef]
54. Du, G.; Dong, W.; Yang, Q.; Yu, X.; Ma, J.; Gu, W.; Huang, Y. Altered Gut Microbiota Related to Inflammatory Responses in Patients With Huntington's Disease. *Front. Immunol.* **2021**, *11*, 603594. [CrossRef]
55. Ellrichmann, G.; Reick, C.; Saft, C.; Linker, R.A. The Role of the Immune System in Huntington's Disease. *Clin. Dev. Immunol.* **2013**, *2013*, 541259. [CrossRef]
56. Katt, M.E.; Mayo, L.N.; Ellis, S.E.; Mahairaki, V.; Rothstein, J.D.; Cheng, L.; Searson, P.C. The Role of Mutations Associated with Familial Neurodegenerative Disorders on Blood–Brain Barrier Function in an IPSC Model. *Fluids Barriers CNS* **2019**, *16*, 20. [CrossRef]
57. Knox, E.G.; Aburto, M.R.; Clarke, G.; Cryan, J.F.; O'Driscoll, C.M. The Blood-Brain Barrier in Aging and Neurodegeneration. *Mol. Psychiatry* **2022**, *27*, 2659–2673. [CrossRef]
58. Hua, J.; Unschuld, P.G.; Margolis, R.L.; van Zijl, P.C.M.; Ross, C.A. Elevated Arteriolar Cerebral Blood Volume in Prodromal Huntington's Disease. *Mov. Disord.* **2014**, *29*, 396–401. [CrossRef]
59. Lin, C.-Y.; Hsu, Y.-H.; Lin, M.-H.; Yang, T.-H.; Chen, H.-M.; Chen, Y.-C.; Hsiao, H.-Y.; Chen, C.-C.; Chern, Y.; Chang, C. Neurovascular Abnormalities in Humans and Mice with Huntington's Disease. *Exp. Neurol.* **2013**, *250*, 20–30. [CrossRef]
60. Vignone, D.; Gonzalez Paz, O.; Fini, I.; Cellucci, A.; Auciello, G.; Battista, M.R.; Gloaguen, I.; Fortuni, S.; Cariulo, C.; Khetarpal, V.; et al. Modelling the Human Blood–Brain Barrier in Huntington Disease. *Int. J. Mol. Sci.* **2022**, *23*, 7813. [CrossRef]
61. Di Pardo, A.; Amico, E.; Scalabrì, F.; Pepe, G.; Castaldo, S.; Elifani, F.; Capocci, L.; De Sanctis, C.; Comerci, L.; Pompeo, F.; et al. Impairment of Blood-Brain Barrier Is an Early Event in R6/2 Mouse Model of Huntington Disease. *Sci. Rep.* **2017**, *7*, 41316. [CrossRef] [PubMed]
62. Yuan, Y.; Sun, J.; Dong, Q.; Cui, M. Blood–Brain Barrier Endothelial Cells in Neurodegenerative Diseases: Signals from the "Barrier". *Front. Neurosci.* **2023**, *17*, 1047778. [CrossRef]
63. Capizzi, M.; Carpentier, R.; Denarier, E.; Adrait, A.; Kassem, R.; Mapelli, M.; Couté, Y.; Humbert, S. Developmental Defects in Huntington's Disease Show That Axonal Growth and Microtubule Reorganization Require NUMA1. *Neuron* **2022**, *110*, e5. [CrossRef] [PubMed]
64. Li, H.; Li, S.-H.; Yu, Z.-X.; Shelbourne, P.; Li, X.-J. Huntingtin Aggregate-Associated Axonal Degeneration Is an Early Pathological Event in Huntington's Disease Mice. *J. Neurosci.* **2001**, *21*, 8473–8481. [CrossRef] [PubMed]
65. Garret, M.; Du, Z.; Chazalon, M.; Cho, Y.H.; Baufreton, J. Alteration of GABAergic Neurotransmission in Huntington's Disease. *CNS Neurosci. Ther.* **2018**, *24*, 292–300. [CrossRef] [PubMed]
66. Bruyn, G.W. Neurotransmitters in Huntington's Chorea—A Clinician's View. *Prog. Brain Res.* **1982**, *55*, 445–464.
67. Horvath, S.; Langfelder, P.; Kwak, S.; Aaronson, J.; Rosinski, J.; Vogt, T.F.; Eszes, M.; Faull, R.L.M.; Curtis, M.A.; Waldvogel, H.J.; et al. Huntington's Disease Accelerates Epigenetic Aging of Human Brain and Disrupts DNA Methylation Levels. *Aging* **2016**, *8*, 1485–1512. [CrossRef] [PubMed]
68. Machiela, E.; Southwell, A.L. Biological Aging and the Cellular Pathogenesis of Huntington's Disease. *J. Huntingt. Dis.* **2020**, *9*, 115–128. [CrossRef]
69. Wang, Y.; Guo, X.; Ye, K.; Orth, M.; Gu, Z. Accelerated Expansion of Pathogenic Mitochondrial DNA Heteroplasmies in Huntington's Disease. *Proc. Natl. Acad. Sci. USA* **2021**, *118*, e2014610118. [CrossRef] [PubMed]

70. Matsushima, A.; Pineda, S.S.; Crittenden, J.R.; Lee, H.; Galani, K.; Mantero, J.; Tombaugh, G.; Kellis, M.; Heiman, M.; Graybiel, A.M. Transcriptional Vulnerabilities of Striatal Neurons in Human and Rodent Models of Huntington's Disease. *Nat. Commun.* **2023**, *14*, 282. [CrossRef]
71. Nopoulos, P.C. Huntington Disease: A Single-Gene Degenerative Disorder of the Striatum. *Dialogues Clin. Neurosci.* **2016**, *18*, 91–98. [CrossRef]
72. Hobbs, N.Z.; Pedrick, A.V.; Say, M.J.; Frost, C.; Dar Santos, R.; Coleman, A.; Sturrock, A.; Craufurd, D.; Stout, J.C.; Leavitt, B.R.; et al. The Structural Involvement of the Cingulate Cortex in Premanifest and Early Huntington's Disease. *Mov. Disord.* **2011**, *26*, 1684–1690. [CrossRef]
73. Lim, R.G.; Al-Dalahmah, O.; Wu, J.; Gold, M.P.; Reidling, J.C.; Tang, G.; Adam, M.; Dansu, D.K.; Park, H.-J.; Casaccia, P.; et al. Huntington Disease Oligodendrocyte Maturation Deficits Revealed by Single-Nucleus RNAseq Are Rescued by Thiamine-Biotin Supplementation. *Nat. Commun.* **2022**, *13*, 7791. [CrossRef]
74. Weinberger, D.R.; Berman, K.F.; Iadarola, M.; Driesen, N.; Zec, R.F. Prefrontal Cortical Blood Flow and Cognitive Function in Huntington's Disease. *J. Neurol. Neurosurg. Psychiatry* **1988**, *51*, 94–104. [CrossRef]
75. Labadorf, A.; Hoss, A.G.; Lagomarsino, V.; Latourelle, J.C.; Hadzi, T.C.; Bregu, J.; MacDonald, M.E.; Gusella, J.F.; Chen, J.F.; Akbarian, S.; et al. RNA Sequence Analysis of Human Huntington Disease Brain Reveals an Extensive Increase in Inflammatory and Developmental Gene Expression. *PLoS ONE* **2015**, *10*, e0143563. [CrossRef] [PubMed]
76. Agus, F.; Crespo, D.; Myers, R.H.; Labadorf, A. The Caudate Nucleus Undergoes Dramatic and Unique Transcriptional Changes in Human Prodromal Huntington's Disease Brain. *BMC Med. Genom.* **2019**, *12*, 137. [CrossRef] [PubMed]
77. Thiruvady, D.R.; Georgiou-Karistianis, N.; Egan, G.F.; Ray, S.; Sritharan, A.; Farrow, M.; Churchyard, A.; Chua, P.; Bradshaw, J.L.; Brawn, T.-L.; et al. Functional Connectivity of the Prefrontal Cortex in Huntington's Disease. *J. Neurol. Neurosurg. Psychiatry* **2007**, *78*, 127–133. [CrossRef]
78. Blumenstock, S.; Dudanova, I. Cortical and Striatal Circuits in Huntington's Disease. *Front. Neurosci.* **2020**, *14*, 82. [CrossRef] [PubMed]
79. Wake, C.; Labadorf, A.; Dumitriu, A.; Hoss, A.G.; Bregu, J.; Albrecht, K.H.; DeStefano, A.L.; Myers, R.H. Novel MicroRNA Discovery Using Small RNA Sequencing in Post-Mortem Human Brain. *BMC Genom.* **2016**, *17*, 776. [CrossRef]
80. Lin, L.; Park, J.W.; Ramachandran, S.; Zhang, Y.; Tseng, Y.T.; Shen, S.; Waldvogel, H.J.; Curtis, M.A.; Richard, R.L.; Troncoso, J.C.; et al. Transcriptome Sequencing Reveals Aberrant Alternative Splicing in Huntington's Disease. *Hum. Mol. Genet.* **2016**, *25*, 3454–3466. [CrossRef]
81. Selemon, L.D.; Rajkowska, G.; Goldman-Rakic, P.S. Evidence for Progression in Frontal Cortical Pathology in Late-stage Huntington's Disease. *J. Comp. Neurol.* **2004**, *468*, 190–204. [CrossRef]
82. Delmaire, C.; Dumas, E.M.; Sharman, M.A.; van den Bogaard, S.J.A.; Valabregue, R.; Jauffret, C.; Justo, D.; Reilmann, R.; Stout, J.C.; Craufurd, D.; et al. The Structural Correlates of Functional Deficits in Early Huntington's Disease. *Hum. Brain Mapp.* **2013**, *34*, 2141–2153. [CrossRef]
83. Andrade-Navarro, M.A.; Mühlenberg, K.; Spruth, E.J.; Mah, N.; González-López, A.; Andreani, T.; Russ, J.; Huska, M.R.; Muro, E.M.; Fontaine, J.-F.; et al. RNA Sequencing of Human Peripheral Blood Cells Indicates Upregulation of Immune-Related Genes in Huntington's Disease. *Front. Neurol.* **2020**, *11*, 573560. [CrossRef]
84. Hensman Moss, D.J.; Flower, M.D.; Lo, K.K.; Miller, J.R.C.; van Ommen, G.-J.B.; 't Hoen, P.A.C.; Stone, T.C.; Guinee, A.; Langbehn, D.R.; Jones, L.; et al. Huntington's Disease Blood and Brain Show a Common Gene Expression Pattern and Share an Immune Signature with Alzheimer's Disease. *Sci. Rep.* **2017**, *7*, 44849. [CrossRef]
85. Mitchell, C.T.; Krier, I.; Arjomand, J.; Borowsky, B.; Tabrizi, S.J.; Leavitt, B.R.; Arran, N.; Axelson, E.; Bardinet, E.; Bechtel, N.; et al. Longitudinal Expression Changes Are Weak Correlates of Disease Progression in Huntington's Disease. *Brain Commun.* **2020**, *2*, fcaa172. [CrossRef] [PubMed]
86. Miller, J.R.C.; Lo, K.K.; Andre, R.; Hensman Moss, D.J.; Träger, U.; Stone, T.C.; Jones, L.; Holmans, P.; Plagnol, V.; Tabrizi, S.J. RNA-Seq of Huntington's Disease Patient Myeloid Cells Reveals Innate Transcriptional Dysregulation Associated with Proinflammatory Pathway Activation. *Hum. Mol. Genet.* **2016**, *25*, 2893–2904. [CrossRef]
87. Ahmad, I.; Singh, R.; Pal, S.; Prajapati, S.; Sachan, N.; Laiq, Y.; Husain, H. Exploring the Role of Glycolytic Enzymes PFKFB3 and GAPDH in the Modulation of Aβ and Neurodegeneration and Their Potential of Therapeutic Targets in Alzheimer's Disease. *Appl. Biochem. Biotechnol.* **2023**, *195*, 4673–4688. [CrossRef] [PubMed]
88. Kee, T.; Khan, S.; Neidhart, M.; Masters, B.; Zhao, V.; Kim, Y.; Percy, K.; Woo, J. The Multifaceted Functions of β-Arrestins and Their Therapeutic Potential in Neurodegenerative Diseases. *Exp. Mol. Med.* **2024**, *56*, 129–141. [CrossRef] [PubMed]
89. Zhou, Y.; Liu, Y.; Peng, Q.; Li, F.; Chen, F. β-Arrestin2 Mediates the Hippocampal Dopaminergic System in Autistic Mouse through the ERK Signaling Pathway. *Behav. Brain Res.* **2022**, *25*, 113888. [CrossRef]
90. Chen, J.; Marks, E.; Lai, B.; Zhang, Z.; Duce, J.A.; Lam, L.Q.; Volitakis, I.; Bush, A.I.; Hersch, S.; Fox, J.H. Iron Accumulates in Huntington's Disease Neurons: Protection by Deferoxamine. *PLoS ONE* **2013**, *8*, e77023. [CrossRef] [PubMed]

91. Wang, K.; Wang, M.; Liao, X.; Gao, S.; Hua, J.; Wu, X.; Guo, Q.; Xu, W.; Sun, J.; He, Y.; et al. Locally Organised and Activated Fth1hi Neutrophils Aggravate Inflammation of Acute Lung Injury in an IL-10-Dependent Manner. *Nat. Commun.* **2022**, *13*, 7703. [CrossRef]
92. Mukherjee, C.; Kling, T.; Russo, B.; Miebach, K.; Kess, E.; Schifferer, M.; Pedro, L.D.; Weikert, U.; Fard, M.K.; Kannaiyan, N.; et al. Oligodendrocytes Provide Antioxidant Defense Function for Neurons by Secreting Ferritin Heavy Chain. *Cell Metab.* **2020**, *32*, 259–272.e10. [CrossRef]
93. Palsa, K.; Baringer, S.L.; Shenoy, G.; Spiegelman, V.S.; Simpson, I.A.; Connor, J.R. Exosomes Are Involved in Iron Transport from Human Blood–Brain Barrier Endothelial Cells and Are Modified by Endothelial Cell Iron Status. *J. Biol. Chem.* **2023**, *299*, 102868. [CrossRef]
94. Jamal, M.H.; Dhupar, M.; Aran, K.R. Exploring the Role of Ferroptosis Pathways in Huntington's Disease: Insight of Pathophysiology to Emerging Treatment. *Brain Disord.* **2025**, *18*, 100207. [CrossRef]
95. Dang, Y.; He, Q.; Yang, S.; Sun, H.; Liu, Y.; Li, W.; Tang, Y.; Zheng, Y.; Wu, T. FTH1- and SAT1-Induced Astrocytic Ferroptosis Is Involved in Alzheimer's Disease: Evidence from Single-Cell Transcriptomic Analysis. *Pharmaceuticals* **2022**, *15*, 1177. [CrossRef] [PubMed]
96. Tian, Y.; Lu, J.; Hao, X.; Li, H.; Zhang, G.; Liu, X.; Li, X.; Zhao, C.; Kuang, W.; Chen, D.; et al. FTH1 Inhibits Ferroptosis Through Ferritinophagy in the 6-OHDA Model of Parkinson's Disease. *Neurotherapeutics* **2020**, *17*, 1796–1812. [CrossRef] [PubMed]
97. Zhou, M.; Xu, K.; Ge, J.; Luo, X.; Wu, M.; Wang, N.; Zeng, J. Targeting Ferroptosis in Parkinson's Disease: Mechanisms and Emerging Therapeutic Strategies. *Int. J. Mol. Sci.* **2024**, *25*, 13042. [CrossRef]
98. Li, X.; Si, W.; Li, Z.; Tian, Y.; Liu, X.; Ye, S.; Huang, Z.; Ji, Y.; Zhao, C.; Hao, X.; et al. MiR-335 Promotes Ferroptosis by Targeting Ferritin Heavy Chain 1 in in Vivo and in Vitro Models of Parkinson's Disease. *Int. J. Mol. Med.* **2021**, *47*, 61. [CrossRef] [PubMed]
99. Bonilla, E.; Estévez, J.; Suárez, H.; Morales, L.M.; de Bonilla, L.C.; Villalobos, R.; Dávila, J.O. Serum Ferritin Deficiency in Huntington's Disease Patients. *Neurosci. Lett.* **1991**, *129*, 22–24. [CrossRef]
100. Morrison, P.J.; Nevin, N.C. Serum Iron, Total Iron Binding Capacity and Ferritin in Early Huntington Disease Patients. *Ir. J. Med. Sci.* **1994**, *163*, 236–237. [CrossRef]

Disclaimer/Publisher's Note: The statements, opinions and data contained in all publications are solely those of the individual author(s) and contributor(s) and not of MDPI and/or the editor(s). MDPI and/or the editor(s) disclaim responsibility for any injury to people or property resulting from any ideas, methods, instructions or products referred to in the content.